

Evaporating Black Hole Interior and Complexity Evolution

Nicolò Bragagnolo and S. Prem Kumar

*Centre for Quantum Fields and Gravity,
Department of Physics,
Swansea University,
Singleton Park, Swansea,
SA2 8PP, U.K.*

E-mail: nicolo.bragagnolo@swansea.ac.uk,
s.p.kumar@swansea.ac.uk

SUMMARY: We study the evolution of the interior of an evaporating black hole in a simple model of Jackiw-Teitelboim (JT) gravity with an end-of-the-world (EoW) brane, where evaporation is modeled by entangling the brane’s internal states with an auxiliary radiation system. To probe the black hole interior, we consider a geodesic length extracted from a boundary-to-brane two-point function and interpret its renormalised value as a measure of subsystem complexity. Our computation, based on quenched disorder averaging, includes non-perturbative gravitational effects from both spacetime wormholes and replica wormholes, encoding ensemble averaging over the dual random Hamiltonian and brane-state couplings. Unlike non-evaporating black holes where complexity first grows linearly and then plateaus at late times $\sim \mathcal{O}(e^{S_{\text{BH}}})$, we find that complexity evolution of the black hole subsystem in the evaporating case differs drastically, depending nontrivially on the dimension of the emitted radiation Hilbert space. It grows linearly at early times, reaches a maximum at Page time $\sim \mathcal{O}(S_{\text{BH}})$, and then decays exponentially. We further show that the relative fluctuations of the interior length remain small before the Page time but become of order one and eventually large at later times: this signals a loss of self-averaging, with the ensemble-averaged complexity dominated by rare configurations rather than by typical realisations.

Contents

1	Introduction	1
2	Setup: JT gravity with EoW brane	5
2.1	Equipping the EoW brane	6
3	Black hole volume/complexity prescription	8
3.1	Length from correlators	8
3.2	Averaging and quenched free energy	9
4	Canonical quantization of JT gravity with EoW brane	11
4.1	Quantising with EoW brane	12
5	Ensemble averaged geodesic length	13
5.1	n -boundary wave function	13
5.2	Quenched average: replica computation	15
5.3	General n result	19
6	Microcanonical ensemble	20
6.1	Kernel $\mathcal{I}(n)$ in microcanonical ensemble	20
6.2	The geodesic length	22
6.2.1	Interior growth rate: fixed k	23
6.2.2	Evaporating scenario: $k \rightarrow k(t)$	23
7	Canonical ensemble	26
7.1	Integral representation of $\mathcal{I}'(0)$	26
7.2	Complexity evolution	27
7.3	Variance of complexity	29
8	Conclusions	30

A	Genus expansion of pure JT gravity	33
B	Partition function JT gravity with EoW brane	34
C	Review of complexity computation in JT with EoW brane	35
D	Page curve	37
E	More on the complexity computation	39
E.1	Truncation of $\exp(\#\omega\beta)$ factors in the kernel $\mathcal{I}(n)$	39
E.2	Computation of $\mathcal{I}(n)$ in the canonical ensemble	40
E.3	Leading contribution of the canonical ensemble computation	43

1 Introduction

The entanglement structure of an evaporating black hole with its emitted Hawking radiation is expected to undergo nontrivial evolution past the Page time of the black hole [1–4]. Within semiclassical gravity, the corresponding changes in entanglement measures is dictated by the appearance of entanglement islands behind the horizon, demarcated by quantum extremal surfaces, accounting for the fact that the semiclassical modes behind the horizon have been radiated away and are in fact contained in the radiation Hilbert space [5–7]. The semiclassical replica wormhole saddle points underlying this picture tell us that insofar as measures of entanglement such as von Neumann and Rényi entropies are concerned, the magnitude of the fluctuations around the classical black hole background, or the Hawking saddle, become large and dominate the contributions to the respective entropies of entanglement.

It is not however immediately clear from these calculations, whether there are significant departures from the classical spacetime geometry behind the horizon in observables unrelated to measures of entanglement.

In this paper we attempt to address this point by examining the volume of the interior of an evaporating black hole within a simple toy model of evaporation which was originally introduced in [6]. Our black hole is described within the effective two dimensional Jackiw-Teitelboim (JT) gravity [8–10] which captures near extremal black hole dynamics. In order to model the entanglement of the black hole with its Hawking quanta, the latter are introduced as an auxiliary reference system R whose

states are maximally entangled with partner states of an end of the world (EoW) brane behind the horizon (see figure 2),

$$|\Psi\rangle = \frac{1}{\sqrt{k}} \sum_{i=1}^k |\psi_i\rangle_B |i\rangle_R, \quad (1.1)$$

where $|\psi_i\rangle_B$ is the state of the black hole B with EoW brane in the state i , and $|i\rangle_R$ is the state of the auxiliary “radiation” system. As the evaporation proceeds, k the dimension of the radiation Hilbert space grows and the naïve or coarse-grained thermal entropy S_{rad} tracks this growth as $k(t) = e^{S_{\text{rad}}(t)}$.

Within this 2d model we will focus attention on a measure of the volume of the black hole interior characterised by the expectation value of a length operator defined via the correlation function of a probe bulk field O_Δ with one insertion at the EoW brane and another at the AdS₂ boundary [11],

$$\langle L(t) \rangle = - \lim_{\Delta \rightarrow 0} \frac{\partial \langle O_\Delta \left(\frac{\beta}{2} + it \right) O_\Delta(0) \rangle}{\partial \Delta}. \quad (1.2)$$

This definition closely parallels that of the length of the Einstein-Rosen bridge in the two-sided AdS₂ black hole [12]. Here Δ denotes the conformal dimension of the boundary operator dual to the bulk operator O_Δ . The definition (1.2) follows intuitively from the observation that the bulk-to-boundary propagator in AdS₂ is $\sim e^{-\Delta L}$ where L is the geodesic distance between the bulk and boundary points. Other prescriptions could in principle be adopted to define the interior length, however (1.2) is a natural one, and has been used to understand the expected behaviour of the quantum complexity of the black hole state or equivalently that of its holographic dual system [13–17]. In the present context, the interior length of the evaporating black hole, appropriately renormalised, must be interpreted as a *subsystem* complexity [18–21].

A distinctive feature of the model we study is that it admits a dual random-matrix description involving both a random Hamiltonian and random couplings specifying the brane states [6]. Correspondingly, the relevant two-point function is obtained from the n -replicated theory, to implement a *quenched disorder average* of the free energy [22, 23] in the presence sources for local operators (cf. eq. (3.13)) and the corresponding geodesic length is extracted by taking the $\Delta \rightarrow 0$ derivative as dictated by eq. (1.2). As a result, the computation of the interior volume receives two conceptually different non-perturbative contributions: ordinary spacetime wormholes, associated with the genus expansion of the pure JT gravitational path integral, and replica wormholes, which arise from the ensemble average over the brane data and encode the correlations responsible for the Page transition.

Our main result is that the interior length as defined above, after appropriate regularisation, interpreted as complexity of an evaporating black hole, behaves quali-

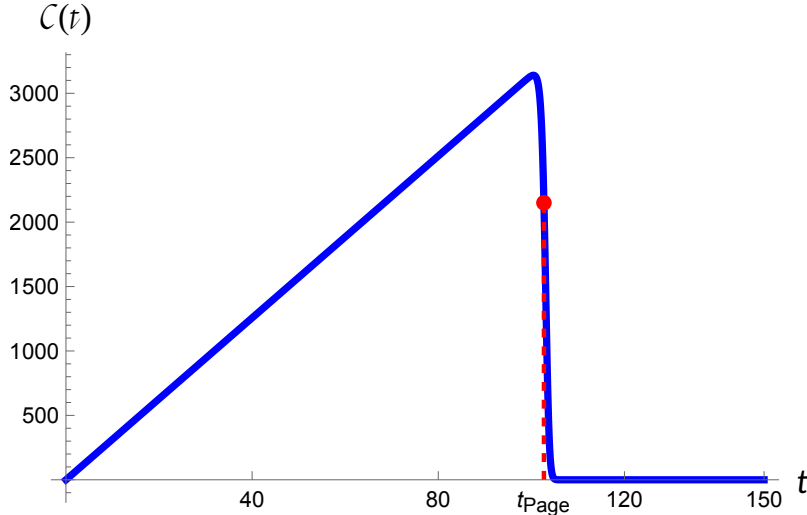


Figure 1: The renormalised geodesic length $\mathcal{C}(t) = \overline{\langle L_{k(t)}(t) \rangle} - \overline{\langle L_{k(t)}(0) \rangle}$ which we identify with the subsystem complexity of the black hole state in the canonical ensemble. We have set $\beta = 0.2$, $S_0 = 8$ and $\dot{S}_{\text{rad}} = 2$ in eq.(7.15) to obtain this plot. The sharp transition (inflection point) happens at Page time $t_{\text{Page}} \simeq 102.7$. Note that we have kept β fixed, while in a realistic setting β must evolve adiabatically with t as well.

tatively differently from that of the non-evaporating AdS black hole. The evaluation of the length is controlled in part by the nonperturbative spectral two-point function of JT gravity [11, 12, 24–26].

Crucially, we find a new nontrivial ingredient in the evaporating case from summing over all replica wormhole contributions, which enters as a kernel in the energy integral that determines the non-perturbative length. The new resummed contributions, denoted $\mathcal{I}(n)$ in the n -replicated theory, arise from summing over all weighted partitions of replica geometries into connected and disconnected multi-boundary components. $\mathcal{I}(n)$ turns out to be a non-monotonic function of $e^{S_{\text{BH}}}/k$, the ratio of the dimensions of the semiclassical black hole and radiation Hilbert spaces. In the microcanonical ensemble, the relevant kernel admits a probabilistic representation,

$$\partial_n \mathcal{I}(n)|_{n=0} = \mathbb{E}_X \left[\frac{X}{(X+1)^2} \right], \quad \text{with } X \sim \text{Poisson} \left(e^{S_{\text{BH}}(t)} - S_{\text{rad}}(t) \right). \quad (1.3)$$

It can be interpreted as the expectation value of the function $f(X) = X/(X+1)^2$ of a Poisson distributed random variable X with mean value $e^{S_{\text{BH}}}/k$. This function has a maximum when $S_{\text{BH}} = S_{\text{rad}} + \mathcal{O}(1)$, making the Page-time crossover especially transparent. We find, both in canonical and microcanonical descriptions, that the renormalised interior length grows linearly at early times and reaches a maximum at a time parametrically close to the Page time. Explicitly, the time evolution of the

renormalised interior length can be summarised as,

$$\overline{\langle L_{k(t)}(t) \rangle}_{\text{ren}} \sim \begin{cases} t, & t \ll t_{\text{Page}}, \\ e^{2(S_{\text{BH}}(t) - S_{\text{rad}}(t))} t, & t_{\text{Page}} \ll t \lesssim e^{S_0}, \end{cases} \quad (1.4)$$

with a further late-time suppression beyond the non-perturbative scale $t \sim e^{S_0}$. Here S_0 is the extremal or zero temperature entropy. Thus, unlike the non-evaporating case where the complexity grows linearly until plateauing at $t \sim e^{S_0}$, the ensemble-averaged complexity of the evaporating black hole turns over near Page time and then decreases exponentially. In the high temperature limit, our result for complexity evolution in the canonical ensemble is particularly simple,

$$\mathcal{C}(t) = \frac{2\pi}{\beta} t \frac{e^{2S_{\text{BH}}(\beta)}}{(k(t) + e^{S_{\text{BH}}(\beta)})^2}, \quad (1.5)$$

and is depicted in figure 1 for $k(t) = e^{S_{\text{rad}}t}$.

A second important result concerns fluctuations. The variance of the interior length can be extracted from the expectation value of the squared geodesic length, and we find the relative magnitude of the fluctuation to be,

$$\frac{\sigma_{\bar{L}}(t)}{\overline{\langle L_{k(t)}(t) \rangle}_{\text{ren}}} \sim \left(\overline{\langle L_{k(t)}(t) \rangle}_{\text{ren}} \right)^{-1/2}. \quad (1.6)$$

This remains parametrically small before Page time, so the ensemble average faithfully captures the behaviour of a typical realization. After the peak, however, the mean length decays exponentially and the relative fluctuations cease to be small: they become order one shortly after the Page-transition time and then grow exponentially. In this sense, the post-Page time regime is characterized by a loss of self-averaging.

The rest of this paper is organised as follows. In section 2 we review JT gravity setup with an EoW brane, and the evaporation model obtained by entangling the brane states with an auxiliary radiation system. In section 3 we explain the replica prescription for the ensemble-averaged boundary-to-brane correlator and its interpretation as a complexity observable. Section 4 reviews the canonical quantization of JT gravity with an EoW brane. Section 5 contains the replica computation of the ensemble-averaged geodesic length. In sections 6 and 7 we study the complexity in the microcanonical and canonical ensembles, respectively, and derive the associated variance. We conclude in section 8 with a discussion of the results and future directions. An extensive appendix is devoted to the technical steps involved in a number of analytical derivations.

2 Setup: JT gravity with EoW brane

Let us review the simple 2d gravity model for an evaporating black hole originally introduced in [6] to derive the Page curve by summing over replica geometries with different topologies. The idea is to consider a two-sided black hole in JT gravity [8–10], with the geometry cut off by an “end-of-the-world brane” (EoW brane) behind the horizon with brane tension μ , which can be viewed as a particle of mass μ [27].

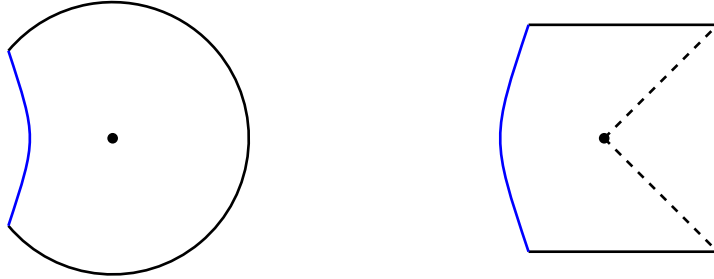


Figure 2: Euclidean (left) and Lorentzian (right) geometries of a black hole with an EoW brane (depicted in blue) behind the horizon.

The overall Euclidean action of the model is given by

$$I_E = I_{\text{JT}} + I_{\text{brane}} \quad (2.1)$$

where the pure JT gravity action including boundary terms is,

$$I_{\text{JT}} = -\frac{S_0}{4\pi} \left(\int_{\mathcal{M}} \sqrt{g} R + 2 \int_{\partial\mathcal{M}} \sqrt{h} K \right) - \int_{\mathcal{M}} \sqrt{g} \phi (R + 2) - 2 \int_{\partial\mathcal{M}} \sqrt{h} \phi (K - 1), \quad (2.2)$$

with $S_0/4\pi$ the extremal entropy of the AdS_2 black hole. The action of the EoW brane with tension μ is of the form

$$I_{\text{brane}} = \mu \int_{\text{brane}} ds. \quad (2.3)$$

As is well known, the equation of motion for the dilaton forces the geometry to be locally AdS_2 , whilst varying with respect to metric yields a nontrivial equation for the dilaton,

$$R + 2 = 0, \quad \nabla_\mu \nabla_\nu \phi - g_{\mu\nu} \nabla^2 \phi + g_{\mu\nu} \phi = 0. \quad (2.4)$$

In addition, both the induced metric and the dilaton value at the asymptotic AdS boundary are fixed as,

$$ds^2|_{\partial\mathcal{M}} = \frac{d\tau^2}{\epsilon^2}, \quad \phi|_{\partial\mathcal{M}} = \frac{\phi_b}{\epsilon}. \quad (2.5)$$

Here $\tau \sim \tau + \beta$ can be interpreted as the periodic Euclidean time of the holographic boundary dual to the JT gravity system and ϵ parametrises the (UV) cutoff scale, the AdS₂ boundary approached in the $\epsilon \rightarrow 0$ limit. For simplicity, we will set the constant $\phi_b = 1$.

Two further boundary conditions must be imposed at the EoW brane,

$$K|_{\text{EoW}} = 0, \quad \partial_n \phi|_{\text{EoW}} = \mu, \quad (2.6)$$

where ∂_n denotes the derivative normal to the EoW brane and K the extrinsic curvature. The vanishing of the extrinsic curvature implies that the EoW brane is a geodesic, whereas the second condition $\partial_n \phi = \mu$ results in vanishing brane Hamiltonian H_{brane} , consistently with gravity being dynamical on the EoW brane [28].

2.1 Equipping the EoW brane

Up to now, the EoW brane is just the geodesic of a particle of mass μ propagating behind the horizon, yielding a \mathbb{Z}_2 quotient of an ordinary two-sided black hole [27].

In order to model the evaporation of the resulting black hole, let us suppose that the EoW brane has a very large number k of possible mutually orthogonal, internal states [6]. The EoW states describe the interior partners of the early Hawking radiation, and these are in turn entangled with an auxiliary system R , which models the early outgoing Hawking radiation of an evaporating black hole. The state of the whole system is given by

$$|\Psi\rangle = \frac{1}{\sqrt{k}} \sum_{i=1}^k |\psi_i\rangle_B |i\rangle_R, \quad (2.7)$$

where $|\psi_i\rangle_B$ is the state of the black hole B with the brane in the state i , and $|i\rangle_R$ is a state of the auxiliary radiation system R .

This model, originally introduced in [6], captures the essential ingredients needed to recover the Page curve of the entropy of the radiation system R using the replica trick. The most direct way to show it is via the study of the purity of the radiation system R . For this, we first introduce the reduced density matrix ρ_R of the radiation system,

$$\rho_R = \frac{1}{k} \sum_{i,j=1}^k |j\rangle \langle i|_R \langle \psi_i | \psi_j \rangle_B \quad (2.8)$$

whose matrix elements $\langle \psi_i | \psi_j \rangle$ are amplitudes between semiclassical gravity states gravity, subject to boundary conditions depicted in figure 3.

The purity of the radiation system R is, by definition,

$$\text{tr}(\rho_R^2) = \frac{1}{k^2} \sum_{i,j=1}^k |\langle \psi_i | \psi_j \rangle|^2. \quad (2.9)$$



Figure 3: Boundary conditions for the computation of $\langle\psi_i|\psi_j\rangle$. The black solid line is the asymptotic boundary with renormalised length β , the arrow represents the direction of time evolution, from the ket to the bra, and at the locations where the dashed blue line labeled by i intersect the solid black line we require that an EoW brane of type i should intersect the asymptotic boundary.

To compute this, we need to consider the boundary conditions associated to the gravity amplitude $|\langle\psi_i|\psi_j\rangle|^2$ and find all the possible ways to “fill them in”. Crucially, there are two different choices: we can either have a disconnected geometry with the topology of two discs, or a connected “Euclidean wormhole” geometry with the topology of a single disc, as illustrated in figure 4.

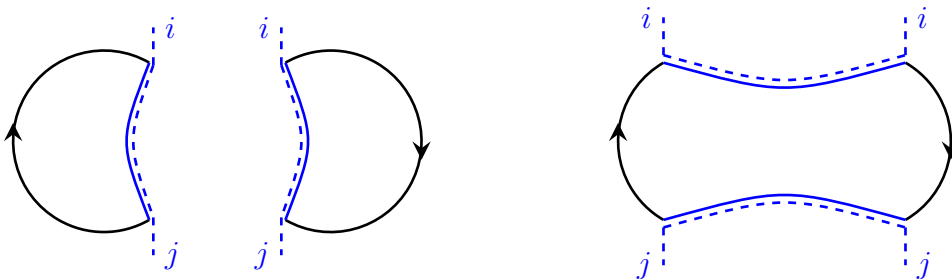


Figure 4: Depiction of the two possible ways of filling in the bulk the boundary conditions of $|\langle\psi_i|\psi_j\rangle|^2$. In order to compute the purity, we sum over the indices i, j by connecting the dashed lines jointly.

To describe the contributions of these geometries to $\text{tr}(\rho_R^2)$, we use the notation $Z_n = Z_n(\beta)$ to represent the gravity path integral on a disc topology with a boundary that consists of alternating segments of n physical boundaries of renormalised lengths β , and n EoW branes. Using this notation, we can evaluate the sum of the two contributions as

$$\text{tr}(\rho_R^2) = \frac{kZ_1^2 + k^2Z_2}{(kZ_1)^2} = \frac{1}{k} + \frac{Z_2}{Z_1^2}. \quad (2.10)$$

In the numerator, we have two contributions: the disconnected one on the left has one k -index loop, and two copies of the geometry that defines Z_1 . The connected contribution has two k -index loops, and a single copy of the geometry corresponding to Z_2 . To obtain the correct normalisation, we finally divide by the gravity result for the square of the trace of the density matrix.

The leading qualitative behaviour of the purity can be captured by retaining only the dependence on the topological S_0 term in the JT gravity action. This term weights the contribution of a topology with Euler characteristic χ , by $e^{S_0\chi}$. Since

the topology relevant for Z_n is disc-like for any value of n , and $\chi = 1$ for the disc, we will have

$$Z_n \propto e^{S_0}. \quad (2.11)$$

Using this formula, (2.10) can be written schematically as

$$\text{tr}(\rho_R^2) = k^{-1} + c e^{-S_0}, \quad (2.12)$$

for some energy and temperature dependent constant c . For small k the disconnected geometry dominates, and the purity scales as $1/k$. For k sufficiently big however, the connected geometry dominates, and the purity $\sim e^{-S_0}$, independent of k . This exchange of dominance of the two saddle-points is the basic mechanism that prevents the entropy (here the 2-Rényi entropy) of the radiation from growing indefinitely.

Using combinatorial arguments it is possible to get the precise evolution of any n -Rényi entropy, including the radiation entanglement entropy. The details of the treatment in the microcanonical ensemble can be found in Appendix D.

3 Black hole volume/complexity prescription

It turns out that pure JT gravity with EoW branes equipped in the way described above is dual to a boundary ensemble of theories, defined by a random Hamiltonian H and a set of brane states $|\psi_i(\beta)\rangle$, which satisfy [6]

$$|\psi_i(\beta)\rangle = \sum_a \Gamma\left(\mu + \frac{1}{2} + i\sqrt{2E_a}\right) e^{-\frac{\beta E_a}{2}} C_{i,a} |E_a\rangle, \quad (3.1)$$

where $|E_a\rangle$ are the eigenstates of the Hamiltonian H and the coefficients $C_{i,a}$ are independent and identically distributed (i.i.d.) complex Gaussian random variables. In the dual random matrix ensemble of this model, the Hamiltonian H can be viewed as a $L \times L$ matrix and C as a $k \times L$ matrix, since the energy and flavor indices assume values $a \in \{1, \dots, L\}$ and $i \in \{1, \dots, k\}$ respectively. The factor of $\Gamma(\mu + \frac{1}{2} + i\sqrt{2E_a})$ originates from an integral over the EoW brane wave function and the Hartle-Hawking state in the geodesic basis [6, 30] which we will review below.

3.1 Length from correlators

A natural proposal for the definition of the expectation value of the geodesic length was identified in [12] in pure JT gravity, extracting it from the two-sided correlator of an operator of dimension Δ . The definition holds on surfaces of arbitrary topology, causing minimal backreaction on the metric and which can be analytically continued between Euclidean and Lorentzian geometries,

$$\langle L \rangle = \lim_{\Delta \rightarrow 0} \left\langle \sum_{\gamma} L_{\gamma} e^{-\Delta L_{\gamma}} \right\rangle, \quad (3.2)$$

where γ labels non self-intersecting geodesics of length L_γ , $\langle \cdot \rangle$ denotes the gravitational path integral summing over hyperbolic surfaces with any topology and Δ acts as a regulator.

For the case of JT gravity with EoW brane (but unequipped with radiation degrees of freedom), in [11] the same procedure as above was applied to extract the value of the geodesic length but now from the *boundary-to-brane* two-point function of a probe matter field O , with scaling dimension Δ as indicated in eq. (1.2).

The two-sided correlation function (1.2) is obtained by analytic continuation from the corresponding Euclidean correlator, computed by summing over all non self-intersecting geodesics connecting the two points, over all surfaces of arbitrary genus.

3.2 Averaging and quenched free energy

The natural extension of the proposal (1.2) to the case of an equipped EoW brane, necessary for mimicking an evaporating black hole, involves considering the ensemble averaged two-point function over the random brane data $\{C_{i,a}\}$, namely

$$\langle O_1 O_2 \rangle \rightarrow \overline{\langle O_1 O_2 \rangle}, \quad (3.3)$$

where $\overline{(\dots)}$ denotes C -averaged quantities. The C -ensemble average of an object X is defined as,

$$\overline{X} = \int dC dC^\dagger P[C, C^\dagger] X, \quad P[C, C^\dagger] \equiv \exp(-\text{Tr}(C^\dagger C)), \quad (3.4)$$

where $P[C, C^\dagger]$ is the average distribution, which is Gaussian by construction.

The un-averaged partition function for gravity plus any matter fields is schematically,

$$Z = \int \mathcal{D}\zeta e^{-I_E}, \quad \mathcal{D}\zeta = \frac{\mathcal{D}g \mathcal{D}\phi}{\text{diffeos}} \quad (3.5)$$

To study correlation functions of operators O_i ,¹ we need to introduce local sources J^i for the operators and work with the generating functional,

$$Z[J^i] = \int \mathcal{D}\zeta e^{-I_E + \sum_i J^i O_i}. \quad (3.6)$$

To obtain the connected correlators, we need its logarithm, the “free energy”,

$$F[J^i] = \log Z[J^i], \quad (3.7)$$

¹The representation of the operators acts non-trivially on the states (3.1).

so n -point correlation functions can be computed as usual,

$$\langle O_1 \cdots O_m \rangle_{\text{conn.}} = \frac{\delta F[J^i]}{\delta J^1 \cdots \delta J^m} \Big|_{J^i=0}. \quad (3.8)$$

Crucially, in a theory of gravity where wormholes may be present, we need the *quenched free energy* since $\overline{\log Z} \neq \log \bar{Z}$ [23] obtained by averaging over the random variables $\{C_{i,a}\}$. This leads us to implement the replica trick for the quenched free energy,

$$\overline{F[J^i]} = \overline{\log Z[J^i]} = \lim_{n \rightarrow 0} \frac{\overline{Z[J^i]^n} - 1}{n} = \lim_{n \rightarrow 0} \frac{\partial \overline{Z[J^i]^n}}{\partial n}. \quad (3.9)$$

Therefore we first consider n copies of the theory to compute $Z[J^i]^n$ and then perform the ensemble average, finally taking the $n \rightarrow 0$ limit. Schematically then, we need to evaluate the ensemble averaged n -replicated partition function:

$$\begin{aligned} \overline{Z[J^i]^n} &= \int dC dC^\dagger P[C, C^\dagger] Z^n[J^i] \\ &= \int dC dC^\dagger P[C, C^\dagger] \int \prod_{A=1}^n \mathcal{D}\zeta_A e^{-\sum_A S_{E,A} + \sum_{A,i} J^i O_{A,i}} \\ &= \int \prod_{A=1}^n \mathcal{D}\zeta_A e^{-S_{E,\text{replica}} + \sum_{A,i} J^i O_{i,A}}, \end{aligned} \quad (3.10)$$

where in the last line we have formally performed the integration over C, C^\dagger , replacing the bulk gravity plus matter action on the replicated geometry, to be viewed as a sum over saddle points. We can finally write

$$\begin{aligned} \overline{\langle O_1 \cdots O_m \rangle_{\text{conn.}}} &= \frac{\delta \overline{F[J^i]}}{\delta J^1 \cdots \delta J^m} \Big|_{J^i=0} \\ &= \lim_{n \rightarrow 0} \frac{\partial}{\partial n} \left\langle \sum_{A=1}^n O_{1,A} \cdots \sum_{B=1}^n O_{m,B} \right\rangle_n \overline{Z[0]^n}, \end{aligned} \quad (3.11)$$

where, on the right hand side, correlation functions are evaluated in the n -replica manifold and include both connected and disconnected contributions. The factor of $\overline{Z[0]^n}$ appears as we are evaluating un-normalised correlators in the replica theory.

Our interest is in the two-point function, with one insertion on the EoW brane and the second on the AdS-boundary:

$$\langle O_1 O_2 \rangle = e^{-\Delta L_{12}}. \quad (3.12)$$

The expectation value of the length operator after the ensemble averaging is,

$$\overline{L_{12}} = - \lim_{\Delta \rightarrow 0} \frac{\partial \overline{e^{-\Delta L_{12}}}}{\partial \Delta} = - \lim_{\Delta \rightarrow 0} \frac{\partial}{\partial \Delta} \left[\lim_{n \rightarrow 0} \frac{\partial}{\partial n} \left\langle \sum_{A=1}^n O_{1,A} \sum_{B=1}^n O_{2,B} \right\rangle_n \overline{Z[0]^n} \right], \quad (3.13)$$

where we will assume that we can interchange the $\Delta \rightarrow 0$ and $n \rightarrow 0$ limits.

Below we will compute this geodesic length between the EoW brane and the asymptotic boundary, and given that the black hole interior volume is a candidate for the quantum complexity, the calculation can be viewed as yielding the complexity evolution for an evaporating black hole. The result will include non-perturbative contributions due to both space-time wormholes and replica wormholes, accounting for the ensemble average over both the Hamiltonian and the EoW brane states respectively.

4 Canonical quantization of JT gravity with EoW brane

In this section we review aspects of canonical quantisation of JT gravity with and without EoW branes, gathering the basic ingredients needed for our calculation.

The canonical quantisation of two-sided JT gravity [29] is in terms of a two-dimensional phase space with canonical variable the renormalised geodesic distance ℓ between the two endpoints of a time slice, and its conjugate momentum P . The Hamiltonian for the system,

$$H = 2 \left(\frac{P^2}{4} + e^{-\ell} \right) \quad (4.1)$$

is that of a non-relativistic particle in an exponential potential. The Hamiltonian is diagonalized by scattering states $|E\rangle$ for $E > 0$, with wavefunctions given by modified Bessel functions,

$$\langle \ell | E \rangle = 4K_{i\sqrt{8E}}(4e^{-\ell/2}) = 4K_{2is}(4e^{-\ell/2}), \quad (4.2)$$

where $s^2 = 2E$, and below it will be convenient to work in these energy units.

The Hartle-Hawking construction provides the natural route for preparing states in the Hilbert space of two-sided JT gravity. Specifically, the key building block is the Hartle-Hawking wavefunction $\Phi_D(\beta, \ell)$, corresponding to the integral over all Euclidean geometries with disc topology bounded by an asymptotic AdS boundary of renormalised length β and a geodesic of length ℓ ,

$$\Phi_D(\beta, \ell) = 4e^{\frac{s_0}{2}} \int_0^\infty ds e^{-\frac{\beta s^2}{2}} \rho_D(s) K_{2is}(4e^{-\ell/2}). \quad (4.3)$$

Here $\rho_D(s)$ is the disc density of states, which is given by [30–32],

$$\rho_D(s) = \frac{s}{2\pi^2} \sinh(2\pi s). \quad (4.4)$$

Upon taking two half discs, each with AdS boundary length $\beta/2$, and sewing them along their geodesic ℓ , we obtain the JT gravity disc partition function,

$$Z_D(\beta) = \int_{-\infty}^{+\infty} d\ell \Phi_D\left(\frac{\beta}{2}, \ell\right) \Phi_D\left(\frac{\beta}{2}, \ell\right) = e^{S_0} \int_0^{+\infty} ds e^{-\frac{\beta s^2}{2}} \rho_D(s). \quad (4.5)$$

4.1 Quantising with EoW brane

The canonical quantization of JT gravity in presence of an EoW brane has been studied in [28]. Similarly to the pure JT gravity case, the Hilbert space can be constructed in terms of L_2 -normalizable functions of L , which represents the renormalised geodesic distance between the AdS boundary and the EoW brane.

The Hamiltonian in this case,

$$H = 2 \left(\frac{P^2}{4} + \mu e^{-L} + e^{-2L} \right), \quad (4.6)$$

corresponds to the quantum mechanics of a particle in a Morse potential. For $\mu = 0$, the Hamiltonian reduces to the one of two-sided JT gravity (4.1) via the identification $\ell = 2L$. This is consistent with having a tensionless EoW brane, cutting the two-sided geometry in two identical halves. Note that for negative tensions, $\mu < 0$ the Hamiltonian becomes negative for L greater than a critical value; whilst remaining bounded from below, it now has bound states corresponding to a naked EoW brane, rather than a black hole. For the rest of this paper, we will assume $\mu > 0$.

Setting $z = 4e^{-L}$, the eigenstates are given by Whittaker functions of second kind

$$\langle L|s\rangle = \sqrt{f_\mu(s)} \frac{W_{-\mu, is}(z)}{\sqrt{z}}, \quad f_\mu(s) = 2\gamma_\mu(s)\rho_D(s), \quad (4.7)$$

where we have defined

$$\gamma_\mu(s) = \left| \Gamma\left(\frac{1}{2} + \mu + is\right) \right|^2. \quad (4.8)$$

The normalisation of the wavefunction (4.7) follows from the following orthogonality relation of the Whittaker functions,

$$\int_0^\infty \frac{dz}{z^2} W_{-\mu, is}(z) W_{-\mu, is'}(z) = \frac{1}{f_\mu(s)} \delta(s - s'). \quad (4.9)$$

Now we can write down the Hartle-Hawking state in the L basis for the one-sided black hole with an EoW brane [11] (without the EoW internal states), as an integral over Euclidean disc topologies enclosed by an asymptotically AdS boundary of renormalised length β , an EoW brane, and a geodesic of length L connecting them:

$$\Psi_D(\beta, L) = \sqrt{2} e^{\frac{s_0}{2}} \int_0^\infty ds e^{-\frac{\beta s^2}{2}} \gamma_\mu(s) \rho_D(s) \frac{W_{-\mu, is}(z)}{\sqrt{z}}. \quad (4.10)$$

The disc partition function is computed as before by sewing two such half-discs,

$$Z_{D, \mu}(\beta) = \int_0^\infty \frac{dz}{z} \Psi_D\left(\frac{\beta}{2}, L\right) \Psi_D\left(\frac{\beta}{2}, L\right) = e^{s_0} \int_0^\infty ds e^{-\frac{\beta s^2}{2}} \gamma_\mu(s) \rho_D(s) \quad (4.11)$$

Including the EoW brane changes the disc density of states,

$$\rho_D(s) \rightarrow \rho_D(s) \left| \Gamma\left(\frac{1}{2} + \mu + is\right) \right|^2, \quad (4.12)$$

modifying the qualitative growth of states large s .

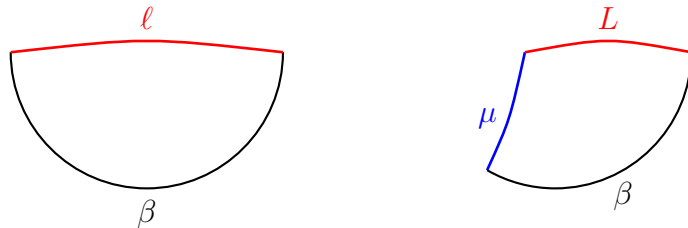


Figure 5: Hartle-Hawking wavefunctions, $\Phi_D(\beta, L)$ for two-sided JT black hole (left) and $\Psi_D(\beta, L)$ for the single-sided JT black hole with an EoW brane (right).

5 Ensemble averaged geodesic length

To compute the geodesic length employing a quenched averaging of $\log Z$, we need to gather the ingredients of the associated replica calculation. Key amongst these is the Hartle-Hawking wave function for the n -boundary geometry to which we first turn our attention.

5.1 n -boundary wave function

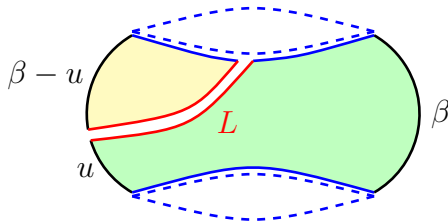


Figure 6: Pictorial representation of the two disc-like geometries associated to the generalized Hartle-Hawking wavefunctions $\Psi_2(\beta + u, L)$ (shaded in green) and $\Psi_1(\beta - u, L)$ (shaded in yellow), whose patch gives the path integral Z_2 . From now on, dashed blue lines stands for identification of EoW brane's flavor indices.

The gravitational path integral on a completely connected disc-like wormhole geometry bounded by n asymptotic boundaries and n EoW branes is given by [6],

$$Z_n = e^{S_0} \int_0^\infty ds \rho_D(s) y(s)^n, \quad y(s) = e^{-\frac{\beta s^2}{2}} \gamma_\mu(s). \quad (5.1)$$

Having n boundaries, each of length β , has the effect of rescaling β by a factor of n , and the introduction of each EoW brane with tension μ is accompanied by a factor of $\gamma_\mu(s)$ in the effective density of states. The corresponding generalised Hartle-Hawking state wave function is,

$$\Psi_n(x, L) = \sqrt{z} e^{\frac{S_0}{2}} \int_0^{+\infty} ds \rho_D(s) e^{-\frac{x s^2}{2}} \gamma_\mu(s)^n \frac{W_{-\mu, is}(z)}{\sqrt{z}}. \quad (5.2)$$

This is the outcome of a gravitational path integral over geometries with n AdS boundaries of total length x , n EoW branes, and one geodesic of length L stretching from an EoW brane to an AdS boundary. In particular, it can be verified that the $n = 2$ partition function Z_2 is obtained by gluing two generalised Hartle-Hawking states, as depicted in figure 6,

$$Z_2 = \int_0^{+\infty} \frac{dz}{z} \Psi_1(\beta - u, L) \Psi_2(\beta + u, L). \quad (5.3)$$

The equality (5.3) follows from the normalization property (4.9) of the Whittaker functions.

The standard procedure for deriving (5.2) is to first consider the gravitational path integral over the disc with $2n + 1$ geodesic boundaries of fixed lengths [6]

$$I_{2n+1}(\ell_1, \dots, \ell_{2n}, \ell_{2n+1}) = 2^{2n+1} \int_0^{+\infty} ds \rho_D(s) \prod_{j=1}^{2n+1} K_{2is}(4e^{-\ell_j/2}). \quad (5.4)$$

This object assumes that each geodesic stretches between two asymptotic AdS₂ boundaries. If we wish to replace one of the geodesics with a geodesic stretching between an asymptotic boundary and an EoW brane, this can be achieved by replacing the corresponding Bessel function with a Whittaker function,

$$I_{2n+1}(\ell_1, \dots, \ell_{2n}, L) \rightarrow 2^{2n-1/2} \int_0^{+\infty} ds \rho_D(s) \prod_{j=1}^{2n} K_{2is}(4e^{-\ell_j/2}) W_{-\mu, is}(4e^{-L/2}). \quad (5.5)$$

To obtain the generalised Hartle-Hawking state Ψ_n with L fixed, we must then integrate over the remaining $2n$ geodesic lengths with a suitable wavefunction for each geodesic, which is either $2^{(1+2\mu)} e^{-(\mu+\frac{1}{2})\ell}$ for an EoW brane² or the disc wavefunction (4.3) $\Phi_D(\beta, \ell)$ to account for an asymptotic AdS₂ boundary.³ This procedure leads to the generalised Hartle-Hawking state in the case with n EoW branes, and n AdS₂ boundaries. Using standard integrals involving the Bessel functions, we find,

$$\begin{aligned} \Psi_n(n\beta, L) &= \quad (5.6) \\ &e^{\frac{S_0}{2}} 2^{(1+2\mu)n} \int \prod_{i=1}^{2n} d\ell_i e^{L/2} I_{2n+1}(\ell_1, \dots, \ell_{2n}, L) \prod_{j=1}^n \left(e^{-\frac{S_0}{2}} \Phi_D(\beta, \ell_j) e^{-(\mu+\frac{1}{2})\ell_{j+1}} \right) \\ &= \sqrt{2} e^{\frac{S_0}{2}} \int_0^{+\infty} ds \rho_D(s) e^{-\frac{n\beta s^2}{2}} \gamma_\mu(s)^n \frac{W_{-\mu, is}(z)}{\sqrt{z}}. \end{aligned}$$

²This wavefunction differs from $e^{-\mu\ell}$, derived in Appendix D of [6], since we chose a different set of brane states $|\psi_i(\beta)\rangle$ (3.1) to make contact with the canonical quantization of JT with EoW brane carried out in [28]. Nonetheless this basis difference, the results of this paper will be independent on it, since we will work either in the microcanonical ensemble or in the large brane mass limit.

³Here we need to be careful to remove the factor of $e^{-S_0/2}$ in (4.3).

Integration over the $2n$ geodesics requires ℓ_j -dependent measure factors [6, 30] which have already been accounted for in arriving at the expression above. Note also that the final result scales with $e^{S_0/2}$ as expected for the disc wave function; factors of $e^{-S_0/2}$ in the first line of (5.6) are needed to strip off the corresponding normalisation in Φ_D as defined in (4.3).

5.2 Quenched average: replica computation

Exploiting the wavefunctions derived above, we want to find a closed form expression for the expectation value of the interior length L in a general replica geometry,

$$\langle L(t) \rangle_n \equiv -\frac{1}{k} \cdot \lim_{\Delta \rightarrow 0} \frac{\partial}{\partial \Delta} \left(\left\langle \sum_{A=1}^n O_{1,A} \sum_{B=1}^n O_{2,B} \right\rangle \overline{Z^n} \right). \quad (5.7)$$

Eventually we will take $n \rightarrow 0$ limit and arrive at the expectation value of the geodesic length,

$$\overline{\langle L(t) \rangle} = \lim_{n \rightarrow 0} \frac{\partial}{\partial n} \langle L(t) \rangle_n. \quad (5.8)$$

We draw attention to the factor of $1/k$ that appears in (5.7). This is an important ingredient in what follows and has implications for the physics we infer. It is required in order to yield the correctly normalised $\langle O_1 O_2 \rangle$ correlator. Since the operators $O_{1,2}$ do not carry any brane/flavour indices, their normalised correlator in the absence of replica wormholes must have no k -dependence, thus the extra factor of $1/k$ is required to ensure that the completely disconnected contributions to our replica correlator do not have any k dependence.

Example $n = 2$: It is instructive first consider the $n = 2$ case to unpack the calculation of $\langle L(t) \rangle_n$ for generic integer n . The un-normalized $n = 2$ replica correlation functions inside the Δ -derivative in (5.7) can be written as

$$\begin{aligned} \left\langle \sum_{A=1}^2 O_{1,A} \sum_{B=1}^2 O_{2,B} \right\rangle \overline{Z^2} &= 2kZ_1 \int_0^\infty \frac{dz}{z} \Psi_1(\beta - u, L) \Psi_1(u, L) \left(\frac{z}{4}\right)^\Delta + \\ &+ 2k^2 \int_0^\infty \frac{dz}{z} \Psi_2(2\beta - u, L) \Psi_1(u, L) \left(\frac{z}{4}\right)^\Delta + \\ &+ 2k^2 \int_0^\infty \frac{dz}{z} \Psi_2(\beta + u, L) \Psi_1(\beta - u, L) \left(\frac{z}{4}\right)^\Delta. \end{aligned} \quad (5.9)$$

The first term accounts for two disconnected copies of the single-disc geometry, with a geodesic constructed in one of them connecting the EoW brane to the AdS boundary. The second and third terms represent geodesic contributions built in the wormhole connected replica geometries (figure 6 and its mirror image). Each contribution is weighted by an appropriate power of k , which counts the number of EoW brane index loops.

Taking the Δ -derivative and following the steps detailed in appendix C, we find,

$$\begin{aligned} \langle L_k(t) \rangle_{n=2} &= L_{k,\text{div}}|_{n=2} \\ &- \frac{2\pi e^{2S_0}}{3k} \int_{E_*}^{\infty} dE \mathcal{I}(n=2) \sqrt{2E} \rho_D(E)^2 \left(1 - \frac{t}{2\pi \rho_D(E) e^{S_0}} \right)^3, \end{aligned} \quad (5.10)$$

where we have introduced a subscript label k for the geodesic length in the theory with k EoW brane states. A noteworthy point which will be important subsequently, is that the divergent contributions from energy integrals depend nontrivially on k and n . As in [11, 12], central to the derivation of this intermediate result is the non-perturbative spectral two-point function in JT gravity (A.7) which includes spacetime wormhole effects joining the two halves of the disc geometries sliced by the geodesic. Crucially, the *new element* in the present context is the kernel $\mathcal{I}(n)$ in the energy integral above, which also includes the effect of replica wormholes on the disc geometries. We describe this in some detail below, first breaking up the individual contributions to $\mathcal{I}(n=2)$ and explaining their combinatorial origin via the generalisation for arbitrary n ,

$$\mathcal{I}(n=2) = e^{-\beta E} \gamma_{\mu}(E) k \times 1 \times 1 \times \binom{2}{1} Z_1 + e^{-2\beta E} \gamma_{\mu}(E)^2 k^2 \times 2 \times 2 \times \binom{2}{2}. \quad (5.11)$$

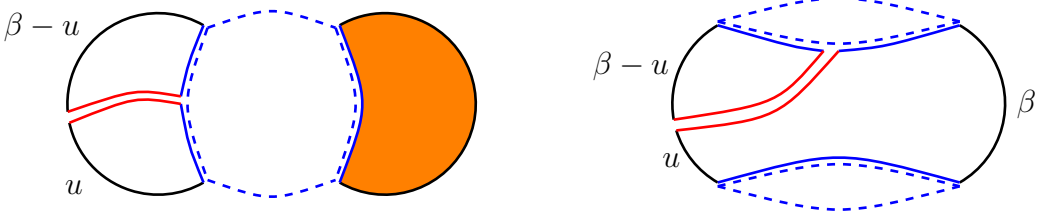


Figure 7: Topologically distinct contributions to $\mathcal{I}(n=2)$.

General n prescription: For general n , we can write,

$$\mathcal{I}(n) = \sum_{j=1}^n \mathcal{I}_j(n), \quad (5.12)$$

where the $\{\mathcal{I}_j\}$ are schematically,

$$\begin{aligned} \mathcal{I}_j(n) = & \underbrace{e^{-j\beta E}}_{\text{boundary weight}} \times \underbrace{\gamma_{\mu}(E)^j}_{\text{brane weight}} \times \underbrace{k^j}_{\text{index loops}} \times \underbrace{j}_{\text{\#geodesics}} \times \underbrace{j}_{\text{\#branes}} \times \underbrace{\binom{n}{j}}_{\text{topology}} \times \underbrace{(\dots)}_{\text{un-sliced pieces}}. \end{aligned} \quad (5.13)$$

geometry sliced by the geodesic

Each $\mathcal{I}_j(n)$ represents a specific topology of the n -replica geometry with a j -boundary⁴ connected component in which the geodesic from an EoW brane resides, accompanied by the remaining components with $(n - j)$ AdS boundaries which can include both connected and disconnected pieces. Since the geodesic slices through the j -boundary connected component we will call this the “sliced” geometry (see figure 7). This is accompanied by a combinatorial factor $\binom{n}{j}$ from picking j out of n boundaries. Each sliced geometry has j -boundaries of total length $j\beta$ which is reflected in the Boltzmann factor $e^{-j\beta E}$ or “boundary weight”. Since there are also j EoW branes, we get a “brane weighting” factor $\gamma_\mu(E)^j$. Every brane boundary is accompanied by an index loop which sums over the k brane states yielding an additional factor of k^j . Finally, within a given sliced geometry, the geodesic can begin at any one of j possible EoW branes and end on any one of j possible AdS boundaries. It is not *a priori* obvious that these different endpoint choices should yield identical contributions, nonetheless they do when the timescales in question are large compared to β , the thermal time, as clarified in a moment.

The “un-sliced” contribution to \mathcal{I}_j is from the path integral over all possible geometries which can be constructed with the remaining $n - j$ asymptotic boundary/EoW brane pairs, along with their respective topology-specific binomial factors and brane index loop factors.

We now make some remarks on the approximations made in getting to eq. (5.10) and the kernel (5.11). Firstly, in the energy integrals arising from the two-point functions, we have worked to leading nontrivial order in the coincidence limit for the spectral two-point functions $\langle \rho(E_1)\rho(E_2) \rangle$, which means that we have worked in the small ω limit ($\omega = E_1 - E_2$) and set contributions $\sim e^{\omega\beta}$ to unity (so $\omega\beta$ is small and the time scales of our interest are much larger than thermal time β). Such terms enter into the boundary weights of generalized Hartle-Hawking wavefunctions (5.2), and yield additional constant contributions to the ω -integrals in (C.9). We have checked the consistency of this truncation in appendix E.1.

Second, we do not consider handles⁵ which increase the genus and are suppressed by powers of e^{-2S_0} , or brane crossing terms which are suppressed by powers of k^{-2} . These would introduce subleading corrections, as was also the case for the derivation of the Page curve within this evaporating black hole model [6, 33]. We also do not include EoW brane loops, since all the brane geodesics must begin and end on an asymptotic AdS boundary. Finally, one may argue that we should also include geodesics not cutting through a disc geometry, rather joining local operator insertions in disconnected geometries. It is unclear how to interpret this physically,

⁴Here we refer to the number of AdS boundaries of the geometry, which also coincides with the number of EoW boundaries.

⁵Apart from the spacetime wormholes connecting the two pieces involved in the geodesic slicing, which we have been accounting for by implementing (C.3).

since the resulting geodesics do not effectively stretch through any bulk geometry, but it can be checked using the boundary particle formalism that such contributions yield time-independent divergent contributions, which can be subtracted away by an appropriate renormalisation prescription.

Example $n = 3$: Below we take the result (5.10) for any positive integer n to find a closed-form of the kernel $\mathcal{I}(n)$. Before turning to this, we glance at $n = 3$ as an additional illustrative example:

$$\mathcal{I}(3) = \mathcal{I}_1(3) + \mathcal{I}_2(3) + \mathcal{I}_3(3), \quad (5.14)$$

where,

$$\mathcal{I}_3(3) = e^{-3\beta E} \gamma_\mu(E)^3 k^3 \times 3 \times 3 \times \binom{3}{3}, \quad (5.15)$$

$$\mathcal{I}_2(3) = e^{-2\beta E} \gamma_\mu(E)^2 k^2 \times 2 \times 2 \times \binom{3}{2} Z_1, \quad (5.16)$$

$$\mathcal{I}_1(3) = e^{-\beta E} \gamma_\mu(E) k \times 1 \times 1 \times \binom{3}{1} (Z_1^2 + k Z_2). \quad (5.17)$$

This case is instructive as it illustrates two types of geodesics that can arise in the

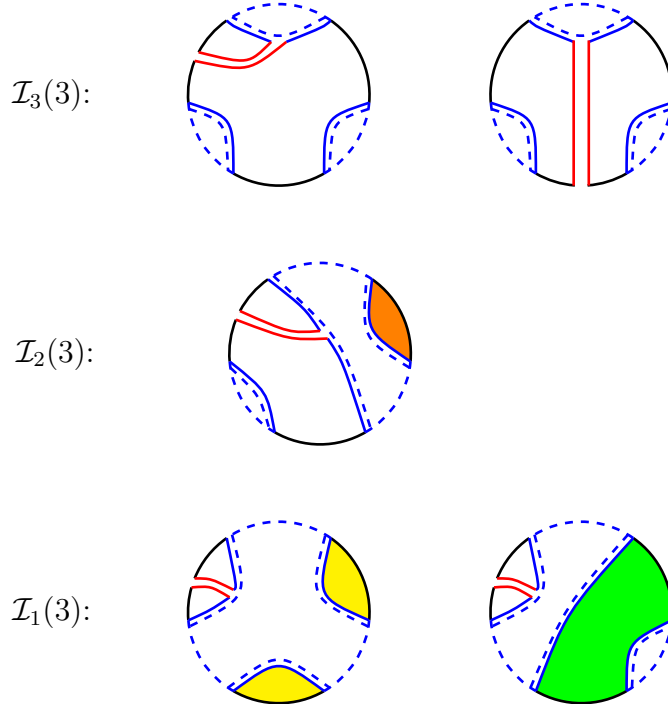


Figure 8: Topologically distinct contributions to the kernel $\mathcal{I}(3)$. The two connected geometries in $\mathcal{I}_3(3)$ sliced through by the geodesic (in red), while topologically the same, differ in the number of boundaries in each slice. Nevertheless they contribute identically to the result.

fully connected sector $\mathcal{I}_3(3)$, given by (5.15), displayed at the top of figure 8. One

slicing divides the geometry into a single AdS boundary half-disc and a 3-boundary half-disc, whilst the second slicing splits it into two 2-boundary states. In the large time regime when the two-point spectral correlator $\langle \rho(E_1)\rho(E_2) \rangle$ is dominated by the coincidence limit $E_1 \rightarrow E_2$, these different configurations yield identical contributions. This is verified explicitly in appendix E.1.

$\mathcal{I}_2(3)$ given by eq. (5.16) accounts for all geodesics built in the second-most connected geometry, consisting of the $j = 2$ replica wormhole, and the un-sliced disconnected disc Z_1 , shaded in orange in figure 8. Finally we have $\mathcal{I}_1(3)$ accounting for all geodesics that can be built cutting through a single disc. In this case the remaining two boundary-brane pairs are either disconnected so we have two discs (Z_1^2 factor shaded yellow in figure 8), or the replica wormhole connected geometry Z_2 (depicted in green in figure 8). The latter has one additional EoW brane flavor loop, explaining the additional factor of k accompanying Z_2 in (5.17).

5.3 General n result

For general n , it is easy to uncover the pattern in the expansion of $\mathcal{I}(n)$. In particular, the combinatorics associated to all ways of partitioning the unsliced portion of the geometry with m boundaries is captured by the m -th complete exponential Bell polynomial [34, 35],⁶

$$B_m(x_1, \dots, x_m) = m! \sum_{\{j_p \geq 0\}} \prod_{p=1}^m \frac{x_p^{j_p}}{(p!)^{j_p} j_p!}, \quad (5.18)$$

with the $\{j_p\}$ constrained so they are associated to partitions of the integer m ,

$$\sum_{p \geq 1} p j_p = m. \quad (5.19)$$

The complete Bell polynomial represents the sum over all ways of partitioning a set of size m into non-empty, unordered subsets of size p and multiplicity j_p , each with weight x_p . In our context the weights x_p must be identified with the connected p -boundary partition function Z_p along with the index loop weighting factor,

$$x_p = k^{p-1} Z_p. \quad (5.20)$$

Recalling from (5.1) that $y(E) \equiv e^{-\beta E} \gamma_\mu(E)$, the kernel $\mathcal{I}(n)$ assumes a compact form in terms of the Bell polynomials,

$$\mathcal{I}(n) = \sum_{p=1}^n y(E)^p k^p p^2 \binom{n}{p} B_{n-p}(k^0 Z_1, k^1 Z_2, \dots, k^{n-p-1} Z_{n-p}). \quad (5.21)$$

⁶The first few Bell polynomials are $B_0 = 1$, $B_1(x_1) = x_1$, $B_2(x_1, x_2) = (x_1^2 + x_2)$, $B_3(x_1, x_2, x_3) = x_1^3 + 3x_1x_2 + x_3$.

However, we still need to understand how to perform the sum and obtain a result analytic in n so that we can evaluate $\mathcal{I}'(0)$, which is in turn required to calculate the expectation value of the length of the black hole interior,⁷

$$\overline{\langle L_k(t) \rangle} = L_{k,\text{div}} - \frac{2\pi e^{2S_0}}{3k} \int_{s_*}^{\infty} ds \frac{\partial \mathcal{I}(n)}{\partial n} \Big|_{n=0} \rho_D^2(s) \left(1 - \frac{st}{2\pi \rho_D(s) e^{S_0}}\right)^3. \quad (5.22)$$

We will address this below, first within the microcanonical ensemble, and then more non-trivially in the canonical picture, finding mutually consistent results.

6 Microcanonical ensemble

Let us first look at the computation of the geodesic length $\overline{\langle L(t) \rangle}$ in the microcanonical ensemble, meaning that we fix the energy in each asymptotic region, rather than fixing the renormalised boundary length β . Specifically, we consider states which have energies in a small band $\Delta E \approx s \Delta s$ with $s = \sqrt{2E}$ fixed. It is then natural to define the microcanonical versions of the entropy and p -boundary partition function which we denote using boldface symbols:

$$e^{\mathbf{S}} = e^{S_0} \rho_D(s) \Delta s, \quad \mathbf{Z}_p = e^{S_0} \rho_D(s) \Delta s y(s)^p, \quad (6.1)$$

where $y(s) = e^{-\beta s^2/2} \gamma_\mu(s)$, so we have the microcanonical relation,

$$\mathbf{Z}_p = e^{\mathbf{S}} y(s)^p. \quad (6.2)$$

6.1 Kernel $\mathcal{I}(n)$ in microcanonical ensemble

Then the complete Bell polynomials, appearing in $\mathcal{I}(n)$ (5.21) are

$$B_{n-p}(\mathbf{Z}_1, k^1 \mathbf{Z}_2, \dots, k^{n-p-1} \mathbf{Z}_{n-p}) = B_{n-p}(a(ky(s)), \dots, a(ky(s))^{n-p}), \quad (6.3)$$

where we have defined,

$$a \equiv \frac{e^{\mathbf{S}}}{k}, \quad (6.4)$$

namely the ratio of the dimensions of the black hole and radiation Hilbert spaces. It is this ratio, more precisely its logarithm, that determines the onset of Page time for an evaporating black hole. The complete Bell polynomials are weighted isobaric polynomials,⁸ which means that the following property holds,

$$B_{n-p}(a(ky), \dots, a(ky)^{n-p}) = (ky)^{n-p} B_{n-p}(a, \dots, a). \quad (6.5)$$

⁷Let us recall $s^2 = 2E$.

⁸An isobaric polynomial is one where each monomial has the same weight (sum of subscript indices).

The complete Bell polynomial B_p with all arguments identical is also known as the Touchard polynomials $T_p(a)$, which admits the following representation [36],

$$T_p(a) = e^{-a} \sum_{r=0}^{+\infty} \frac{a^r r^p}{r!}. \quad (6.6)$$

This displays an immediate relation to the Poisson distribution. $T_p(a)$ is the p -th moment of a Poisson distributed random variable with mean value a : $T_p(a) = \mathbb{E}[X^p]$, $X \sim \text{Poisson}(a)$.⁹ With these ingredients in place, the kernel $\mathcal{I}(n)$ simplifies considerably,

$$\mathcal{I}(n) = n (ky(s))^n e^{-a} \sum_{r=0}^{+\infty} \left[\frac{a^r}{r!} \frac{r^n (n+r)}{(1+r)^{2-n}} \right]. \quad (6.7)$$

Viewing $\mathcal{I}(n)$ as an analytic function of n , $\mathcal{I}'(0)$ is then straightforward to evaluate as an infinite sum¹⁰ which can in turn be expressed in terms of the exponential integral function,

$$\left. \frac{\partial \mathcal{I}(n)}{\partial n} \right|_{n=0} = \frac{e^{-a}}{a} (e^a + \gamma - \text{Ei}(a) + \log a - 1), \quad (6.8)$$

where γ is the Euler-Mascheroni constant. Equivalently, utilising the series representation of the right hand side, $\mathcal{I}'(0)$ can be viewed as the expectation value of the function $f(X) = X/(1+X)^2$ of a Poisson distributed random variable X with mean value a ,

$$\mathcal{I}'(0) = \mathbb{E} \left[\frac{X}{(1+X)^2} \right], \quad X \sim \text{Poisson}(a). \quad (6.9)$$

The most interesting feature of $\mathcal{I}'(0)$ as a function of the ratio a , is that it is a non-monotonic function with a maximum at $a_{\max} \approx 2.306$. This is when the radiation and entropy are essentially equal i.e. $\mathbf{S} = \log k + \mathcal{O}(1)$ and therefore should be identified with the onset of Page time up to small corrections. Whilst k is just a tunable parameter from the perspective of the EoW brane model, in an evaporating black hole, the semiclassical radiation entropy $S_{\text{rad}} = \log k$ grows linearly with time. Therefore, $\log k$ should be viewed as a proxy for time in a slowly evaporating black hole. We will be more precise about this below.

⁹Touchard polynomials have already appeared as moments of a partition-like random variable counting the dimension of asymptotically AdS Hilbert space in the topological toy model studied in [37].

¹⁰The sum in question is $\mathcal{I}'(0) = e^{-a} \sum_{r=0}^{+\infty} \left[\frac{a^r}{r!} \frac{r}{(1+r)^2} \right]$.

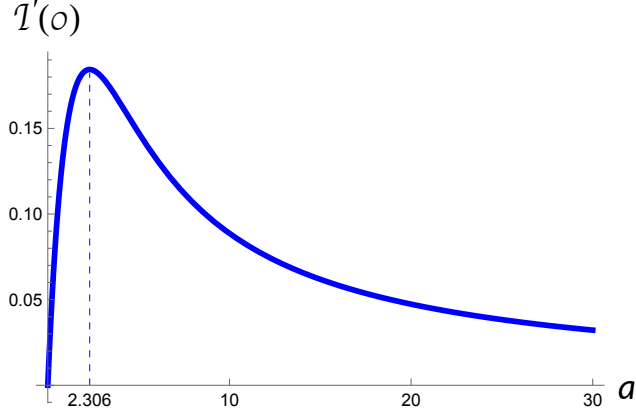


Figure 9: $\mathcal{I}'(0)$ as a function of the ratio $a = e^{\mathbf{S}}/k$.

The asymptotic expansions of $\mathcal{I}'(0)$ for small and large a ,¹¹ yield the following pre-Page and post-Page time (“time” refers to $\log k$) behaviours,

$$\left. \frac{\partial \mathcal{I}(n)}{\partial n} \right|_{n=0} \simeq \begin{cases} \frac{k}{e^{\mathbf{S}}} + \mathcal{O}(k^2 e^{-2\mathbf{S}}) + \mathcal{O}\left(e^{-\frac{e^{\mathbf{S}}}{k}} (\mathbf{S} - \log k) k e^{-\mathbf{S}}\right) & e^{\mathbf{S}} \gg k, \\ \frac{e^{\mathbf{S}}}{4k} + \mathcal{O}(e^{2\mathbf{S}} k^{-2}) & e^{\mathbf{S}} \ll k. \end{cases} \quad (6.12)$$

6.2 The geodesic length

Now let us understand what this means for the expectation value of the geodesic length in the microcanonical ensemble. In practice, this means restricting the energy integral (5.22) to the narrow energy window of $\delta E \approx s \Delta s$, and noting also that the integral has non-vanishing support only when $s > s_*(t)$,

$$\overline{\langle L_k(t) \rangle} = L_{k,\text{div}} - \frac{2\pi}{3} \Theta(s - s_*(t)) \left. \frac{\partial \mathcal{I}(n)}{\partial n} \right|_{n=0} \frac{e^{\mathbf{S}} a}{\Delta s} \left(1 - \frac{s \Delta s t}{2\pi e^{\mathbf{S}}}\right)^3. \quad (6.13)$$

¹¹Near $a = 0$, $\mathcal{I}'(0)$ is regular and admits a power series expansion:

$$\mathcal{I}'(0)|_{a \ll 1} = \frac{a}{4} - \frac{5a^2}{36} + \mathcal{O}(a^3). \quad (6.10)$$

The large a behaviour on the other hand, apart from the leading $1/a$ term, is dictated in part by the asymptotic series for $\text{Ei}(a)$,

$$\mathcal{I}'(0)|_{a \gg 1} = \frac{1}{a} - \sum_{p=0}^{\infty} \frac{p!}{a^{p+2}} + e^{-a} (\log a - 1 + \gamma)/a. \quad (6.11)$$

For $t \gg e^{S_0}$, it follows that $s_*(t) \rightarrow +\infty$,¹² and the time dependent piece vanishes. In the canonical ensemble, the integrand vanishes exponentially as $s \rightarrow +\infty$, so this is smoothly implemented without any step functions. The length as defined has an additive ambiguity, and a natural renormalisation prescription which resolves these ambiguities is the one proposed in [12],

$$\overline{\langle L_k(t) \rangle}_{\text{ren}} = \overline{\langle L_k(t) \rangle} - \overline{\langle L_k(0) \rangle}. \quad (6.14)$$

6.2.1 Interior growth rate: fixed k

One of the most striking consequences of (6.13) is the effect of k on the rate of growth of the interior at early times. This is given by the term linear in t and is the “velocity” of growth,

$$v_k(t) \equiv \left. \frac{d}{dt} \overline{\langle L_k(t) \rangle}_{\text{ren}} \right|_{t \ll e^{S_0}} = \mathcal{I}'(0) a s = \begin{cases} s & k = \mathcal{O}(1) \\ s \frac{e^{2S}}{4k^2} & e^S \ll k. \end{cases}. \quad (6.15)$$

It is easily seen in the canonical ensemble at temperature β^{-1} that $s \approx 2\pi/\beta$. Therefore, as the dimension k of the auxiliary Hilbert space is cranked up, the growth rate of the black hole interior decreases and becomes vanishingly small when the radiation Hilbert space is much larger than the black hole Hilbert space. This is a nontrivial consequence of entangling the black hole/EoW brane system with an auxiliary radiation system.

6.2.2 Evaporating scenario: $k \rightarrow k(t)$

Now let us turn to the implications of (6.13) for an evaporating black hole with k a function of time. It is natural to assume that the system, for most times, evolves adiabatically so that a quasi-static or quasi-equilibrium picture applies. The outgoing radiation can be approximated by a thermal spectrum at the instantaneous Hawking temperature $\beta^{-1}(t)$, while the radiation Hilbert space $k(t)$ can be expressed in terms of the *semiclassical* Hawking radiation entropy $S_{\text{rad}}(t)$ as

$$k \rightarrow k(t) = e^{S_{\text{rad}}(t)}. \quad (6.16)$$

For instance, we can assume that the radiation bath is a $(1+1)$ -d CFT with central charge c , and the entropy flux of radiation assumes the universal form (see e.g. [38])

$$\dot{S}_{\text{rad}}(t) = \frac{\pi c}{6\beta(t)}, \quad (6.17)$$

¹²We recall $s_*(t) = \frac{1}{2\pi} \sinh^{-1} 2\pi t$ which diverges logarithmically at late times, as reviewed in Appendix C.

under the adiabatic condition $|\dot{\beta}(t)| \ll 1$, so one can then write,

$$S_{\text{rad}}(t) \simeq \dot{S}_{\text{rad}} t. \quad (6.18)$$

Given the above picture, we will assume that time evolution in a dynamical setting can be captured by a sequence of fixed- k, β models, with the sequence of parameter values chosen to mimic the expected semiclassical time evolution.

Then we naturally expect that the renormalised geodesic length operator is obtained from (6.14) by the replacement $k \rightarrow k(t)$,

$$\overline{\langle L_{k(t)}(t) \rangle}_{\text{ren}} = \overline{\langle L_{k(t)}(t) \rangle} - \overline{\langle L_{k(t)}(0) \rangle}. \quad (6.19)$$

In this instance, it is worth remarking that the prescription is not just a choice but in fact forced upon us. The reason is that divergent contributions $L_{k,\text{div}}$ in (6.13) depend nontrivially on k and \mathbf{S} which will both be time dependent in the sense explained above, and we must therefore regulate the divergences at each time step of evaporation. The obvious choice would have been to subtract off the length at $t = 0$, $L_{k(0)}(0)$, however this would fail to work at times $t > 0$ when $k \neq k(0)$.

Since the interior volume of the black hole is expected to be a measure of the quantum complexity of the state, we propose that our renormalised length at time t corresponds to the quantum complexity of the evaporating black hole subsystem,

$$\mathcal{C}(t) = \overline{\langle L_{k(t)}(t) \rangle}_{\text{ren}}. \quad (6.20)$$

For the moment we self-consistently focus attention on the early time regime i.e. $t \ll e^{S_0}$, so we write,

$$\mathcal{C}(t) = s \frac{e^{\mathbf{S}}}{k(t)} \frac{\partial \mathcal{I}(n)}{\partial n} \Big|_{n=0} t, \quad t \ll e^{S_0}. \quad (6.21)$$

Expanding $\mathcal{I}'(0)$ as a function of $a = e^{\mathbf{S}}/k$ for $a \gg 1$, keeping the leading and first sub-leading corrections we find that $\mathcal{C}(t)$ starts growing linearly at first, but then reaches a maximum at $t = t_{\text{max}}$,

$$\dot{\mathcal{C}}(t_{\text{max}}) = 0, \quad t_{\text{max}} \simeq \frac{\mathbf{S} - \log \mathbf{S}}{\dot{S}_{\text{rad}}}. \quad (6.22)$$

This is a striking result. Beyond this point, the complexity undergoes a sharp transition to exponential decay around,

$$t \simeq \frac{\mathbf{S} + \mathcal{O}(1)}{\dot{S}_{\text{rad}}}, \quad (6.23)$$

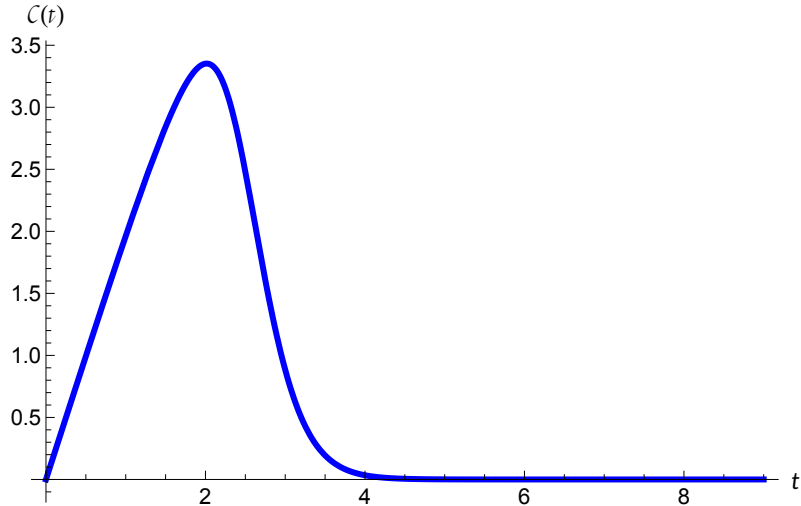


Figure 10: The renormalised geodesic length $\mathcal{C}(t) = \overline{\langle L_{k(t)}(t) \rangle} - \overline{\langle L_{k(t)}(0) \rangle}$ in the microcanonical ensemble, where $S_{\text{BH}}=6$ and $S_{\text{rad}}(t) = \dot{S}_{\text{rad}}t$ with $\dot{S}_{\text{rad}} = 2$. The geodesic length grows linearly, undergoes a transition (inflection point) at the Page time $t_{\text{Page}} = S_{\text{BH}}/\dot{S}_{\text{rad}} = 3$ and decays exponentially.

which is an inflection point and can be identified with the Page time. The complete picture of the time evolution of $\mathcal{C}(t)$ can be summarized as below:

$$\mathcal{C}(t) \simeq \begin{cases} st & t \ll t_{\text{Page}} \\ st e^{2(\mathbf{S} - \dot{S}_{\text{rad}} t)} & t_{\text{Page}} \ll t \lesssim e^{S_0} \\ \frac{\pi}{6\Delta_s} e^{2(\mathbf{S} - \dot{S}_{\text{rad}} t) + \mathbf{S}} & t \gg e^{S_0} . \end{cases} \quad (6.24)$$

It is worth emphasizing that what we are computing here is a candidate *subsystem* complexity, via the non-perturbative evaluation of the interior length. The results above are consistent with the recent findings on subsystem complexity [39, 40]. Before Page time, since the black hole is the larger of the two subsystems its complexity grows linearly, which is consistent with the expectation for early time growth of the complexity of the larger subsystem in a bipartitioned system. We have also found that the rate of this linear growth is bounded from above by that of the non-evaporating black hole [12] (the latter reviewed in Appendix C). The subsystem complexity of the evaporating black hole reaches a maximum just before the Page time, when the Hilbert space dimensions of the black hole and radiation become comparable, following which we see smooth exponential decrease. The drop is due to the fact that the black hole state becomes closer and closer to a maximally mixed state, which is simple, and contains almost no information. The smooth post-Page time decrease is one of two possible conjectured scenarios [40], the other being an abrupt fall to zero, and is potentially a signature of the fact that the entanglement wedge of the black hole does not change abruptly.

7 Canonical ensemble

We would like to now corroborate our observations based on the microcanonical treatment with a complete analysis of the geodesic integral (5.22) in the canonical ensemble. This will be a two step process – first, obtaining an integral representation for the kernel $\mathcal{I}'(0)$ and then employing a saddle-point method to evaluate the renormalised length/complexity.

7.1 Integral representation of $\mathcal{I}'(0)$

In the canonical ensemble, we need to work with the multi-boundary partition functions (5.1) which we now write as,

$$Z_p = e^{S_0} \hat{Z}_p, \quad \hat{Z}_p \equiv \int_0^\infty ds \rho_D(s) y(s)^p, \quad (7.1)$$

and introduce the parameter,

$$a_0 \equiv \frac{e^{S_0}}{k}, \quad (7.2)$$

With these rescalings we can exploit the isobaric property (6.5) of Bell polynomials to write the kernel $\mathcal{I}(n)$ as (E.6), and to show (appendix E.2) that $\mathcal{I}(n)$ is the coefficient of z^n in the series expansion of an analytic function of z ,

$$\mathcal{I}(n) = [z^n] e^{y(s)z} y(s) z(1 + y(s)z) B(z), \quad (7.3)$$

where $B(z)$ is the generating function for the complete Bell polynomials,

$$B(z) = \exp \left(a_0 \sum_{p=1}^{\infty} \hat{Z}_p \frac{z^p}{p!} \right) = \sum_{p=0}^{\infty} B_p(a_0 \hat{Z}_1, \dots, a_0 \hat{Z}_p) \frac{z^p}{p!}. \quad (7.4)$$

After some work, we arrive at an integral representation for $\mathcal{I}'(0)$ which will play a key role in our saddle point evaluation,

$$\begin{aligned} \left. \frac{\partial \mathcal{I}(n)}{\partial n} \right|_{n=0} &= y(s) \int_0^\infty d\chi (1 - \chi y(s)) e^{-\chi y(s)} e^{-a_0 \Phi(\chi)} \\ \Phi(\chi) &= \int_0^\infty ds \rho_D(s) (1 - e^{-\chi y(s)}). \end{aligned} \quad (7.5)$$

Recall from (5.1) that $y(s)$ is the Boltzmann factor times $\gamma_\mu(s)$, the modification in the density of states introduced by the EoW branes (4.8).

7.2 Complexity evolution

Let us return to the expression for the unrenormalised geodesic length,

$$\overline{\langle L_k(t) \rangle} = L_{k,\text{div}} - \frac{2\pi e^{S_0} a_0}{3} \int_{s_*}^{\infty} ds \mathcal{I}'(0) \rho_D^2(s) \left(1 - \frac{st}{2\pi \rho_D(s) e^{S_0}} \right)^3. \quad (7.6)$$

Our microcanonical analysis has already revealed that the early-time regime $t \ll e^{S_0}$, is the really interesting epoch for the evolution of the interior length. Retaining only the linear term in t in the integrand, our prescription (6.20) for the renormalised length or complexity gives,

$$\mathcal{C}(t) = t a_0 \int_0^{\infty} ds s \rho_D(s) \mathcal{I}'(0), \quad t \ll e^{S_0}. \quad (7.7)$$

To stay in an analytically tractable regime, we choose to work in the semiclassical or high temperature limit with $\beta \ll 1$, and further take the brane tension to be large $\mu \gg 1/\beta$. Then, following (B.3),

$$y(s) \approx y(0) \hat{y}(s), \quad y(0) \equiv \mu^{2\mu}, \quad \hat{y}(s) \equiv e^{-\frac{\beta s^2}{2}}. \quad (7.8)$$

Since the integrand in our integral representation (7.5) for $\mathcal{I}'(0)$ only depends on the combination $\chi y(s)$, it is natural to absorb the factor of $y(0)$ into χ via the integration variable change $u = y(0)\chi$:

$$\mathcal{I}'(0) = \hat{y}(s) \int_0^{\infty} du (1 - u\hat{y}(s)) e^{-u\hat{y}(s)} e^{-a_0\Phi(u)}, \quad u \equiv \chi y(0). \quad (7.9)$$

Likewise,

$$\Phi(u) = \int_0^{\infty} ds' \rho_D(s') \left(1 - e^{-u\hat{y}(s')} \right). \quad (7.10)$$

We note that $\Phi(u)$ is a non-negative, monotonically increasing function of u . In addition, $\Phi(0) = 0$, hence for small u it is linear,

$$\Phi(u) \approx \Phi'(0)u, \quad \Phi'(0) = \hat{Z}(\beta) = \frac{e^{\frac{2\pi^2}{\beta}}}{\sqrt{2\pi} \beta^{3/2}}. \quad (7.11)$$

In the linearised limit, the integrand is Gaussian and dominated by the saddle at $s_0 = 2\pi/\beta$, so we may naïvely expect the linear behaviour to hold for $u\hat{y}(s_0) \ll 1$, or $u \ll e^{2\pi^2/\beta}$.¹³ Note that $\Phi'(0)$ is the disc partition function of JT gravity evaluated at the saddle. In the high temperature limit

$$\Phi'(0) \sim e^{2\pi^2/\beta} \gg 1. \quad (7.12)$$

¹³The series expansion for $\Phi(u) = \frac{1}{\sqrt{2\pi}\beta^{3/2}} \sum_{n=1}^{\infty} (-1)^{n+1} \frac{u^n}{n!n^{3/2}} e^{2\pi^2/n\beta}$ is absolutely convergent.

This has an important consequence for $\mathcal{I}'(0)$ in (7.9). In the linear regime for $\Phi(u)$, the integrand has a sharp maximum at,

$$u_{\max} = \frac{1}{\hat{y}(s) + a_0 \Phi'(0)}. \quad (7.13)$$

Given that $\hat{y}(s) \leq 1$, it is guaranteed for $a_0 \sim \mathcal{O}(1)$, that $u_{\max} \sim \mathcal{O}(e^{-2\pi^2/\beta})$ and therefore the linear approximation for $\Phi(u)$ will work exceedingly well in the high temperature limit. However, as we approach Page time $a_0 \sim \mathcal{O}(e^{-4\pi^2/\beta})$, $u_{\max} \sim \mathcal{O}(e^{2\pi^2/\beta})$ which is close to the edge of validity of the linear approximation for $\Phi(u)$. At this point we must consider the effects outside the linear regime, as in Appendix E.3 and we find that they remain subleading at all times. Therefore, we find

$$\mathcal{I}'(0) \approx \frac{a_0 \hat{y}(s) \Phi'(0)}{(\hat{y}(s) + a_0 \Phi'(0))^2}. \quad (7.14)$$

The denominator is a very slowly varying function of s since $\hat{y}(s)$ is bounded below unity, whilst the numerator is a Gaussian. Therefore $\mathcal{C}(t)$ can be evaluated readily by performing the Gaussian integral and evaluating the denominator at the saddle point,

$$\boxed{\mathcal{C}(t) = \frac{2\pi}{\beta} t \frac{e^{2S_{\text{BH}}(\beta)}}{(k(t) + e^{S_{\text{BH}}(\beta)})^2}}. \quad (7.15)$$

Here we used the fact that the log-corrected Bekenstein-Hawking entropy of a black hole in JT gravity [10] is,¹⁴

$$S_{\text{BH}}(\beta) \simeq S_0 + \frac{4\pi^2}{\beta} - \frac{3}{2} \log \beta, \quad (7.16)$$

and we have restored $a_0 = e^{S_0}/k$ and in the dynamical situation the explicit time dependence of the radiation Hilbert space dimension $k(t) = e^{S_{\text{rad}}(t)}$. Indeed, in order to apply this to a slowly evaporating near extremal black hole we must also replace β with $\beta(t)$ in accordance with black hole thermodynamics and energy conservation. Given our present setup, we will reserve further detailed study of the full dynamical setting for future work.

Some comments on (7.15) are in order. Remarkably, (7.15) is precisely reproduced by our microcanonical result (6.21) by replacing the Poisson random variable X by its mean

$$\mathbb{E}_{a(t)} \left[\frac{X}{(1+X)^2} \right] \rightarrow \frac{a(t)}{(1+a(t))^2} \quad \Longrightarrow \quad \mathcal{C}(t)|_{\text{micro}} \rightarrow \mathcal{C}(t)|_{\text{can}} \quad (7.17)$$

¹⁴Let us recall that we have set $\phi_b = 1$ and $8\pi G_N = 1$ from the outset.

where $a(t) = e^{S_{\text{BH}}}/k(t)$. This replacement is justified at early, pre-Page times, where $a(t) \gg 1$. Indeed, the ratio of the standard deviation value and the mean is $1/\sqrt{a}$ for a Poisson variable, thus the distribution of X becomes sharply localised around its mean, and the microcanonical average reduces to the canonical result. The post-Page time evolution, as we elaborate on further below, will see large fluctuations.

In the non-dynamical setting, dialing k reduces the rate of complexity growth or the “velocity” from $2\pi/\beta$ for small k to $\sim e^{2S_{\text{BH}}}/k^2$ for large k exactly as we found in the microcanonical ensemble. The time evolution of (7.15) is also consistent with the behaviour found in the microcanonical ensemble. In particular, we find a peak at time,

$$t_{\text{peak}} \simeq \frac{S_{\text{BH}}(\beta) - \log S_{\text{BH}}(\beta)}{\dot{S}_{\text{rad}}}, \quad (7.18)$$

and a sharp transition (inflection point) at Page time,

$$t_{\text{Page}} \simeq \frac{S_{\text{BH}}(\beta)}{\dot{S}_{\text{rad}}}. \quad (7.19)$$

7.3 Variance of complexity

The variance of complexity can be characterized via

$$\sigma_L^2 = \overline{\langle L_k(t)^2 \rangle} - \overline{\langle L_k(t) \rangle}^2 = \overline{\langle L_k(t)^2 \rangle}_{\text{conn.}} \quad (7.20)$$

where the subscript denotes that only connected two-point functions are taken into account in the evaluation of the expectation value of the geodesic length squared. Exploiting the identity

$$L^2 = \log^2(e^{-L}) = \lim_{\Delta \rightarrow 0} \frac{\partial^2}{\partial \Delta^2} e^{-\Delta L}, \quad (7.21)$$

it is straightforward to get the variance of complexity simply by following the same procedure based on the two-point function computation. Taking the second derivative of $\mathcal{M}(\Delta, E_1, E_2)$ in (C.2) with respect to Δ yields,

$$\lim_{\Delta \rightarrow 0} \frac{\partial^2}{\partial \Delta^2} \mathcal{M}(\Delta, E_1, E_2) = \frac{\sqrt{2E}}{2\pi\gamma_\mu(E)\rho_D(E)} \frac{F(E, \mu)}{\omega^2} + \mathcal{O}(\omega^{-1}), \quad (7.22)$$

in $E_1 \rightarrow E_2$ limit with $\omega = E_1 - E_2$. Thus, we can conclude that the ω -integral in (C.8) remains unchanged and we get an additional function $F(E, \mu)$, containing hypergeometric and polygamma functions, in the final energy integral. For large brane tension $\mu \gg 1/\beta$ limit, the new factor $F(E, \mu)$ simplifies considerably,

$$F(E, \mu) \simeq -2(\gamma + \log 4) + \psi(2i\sqrt{2E}) + \psi(-2i\sqrt{2E}). \quad (7.23)$$

We find that the resulting noise to signal ratio, or the relative fluctuation of the interior length obeys,

$$\frac{\sigma_{\bar{L}}}{\langle L_{k(t)}(t) \rangle_{\text{ren}}} \simeq \sqrt{\frac{2 \log(\beta^{-1})}{\langle L_{k(t)}(t) \rangle_{\text{ren}}}}. \quad (7.24)$$

Consequently, for early times $t \lesssim t_{\text{Page}}$ the relative fluctuations are parametrically small, scaling as $\beta^{1/2} \log^{1/2}(\beta^{-1}) t^{-1/2}$. After the complexity peak, i.e. once the black hole interior starts to decay exponentially, the absolute fluctuations are exponentially suppressed as well, yet the relative fluctuations cease to be negligible. The latter becomes $\mathcal{O}(1)$ shortly after the Page-transition time and then exponentially increases. One possible reason to explain this behaviour can be found by looking back at the microcanonical ensemble result: the complexity is controlled by an expectation value of a bounded nonlinear function of a Poisson-distributed variable X with exponentially decaying mean (6.9), and it turns out that the post-Page-time expectation value is dominated by exponentially rare configurations $X \simeq 1$. As a result, while the ensemble-averaged complexity decays exponentially, its relative fluctuations grow exponentially, signaling a loss of typicality.

8 Conclusions

In this work we studied the evolution of the interior of an evaporating black hole in JT gravity with an end-of-the-world brane. Evaporation was modelled by entangling the internal states of the brane with an auxiliary radiation system, whose Hilbert space grows during the evaporation process. We probed the black hole interior through a boundary-to-brane two-point function and extracted from it a renormalised geodesic length, which we interpreted as a candidate measure of the subsystem complexity of the evaporating black hole.

The main new ingredient in the computation is the quenched ensemble average over the brane data. This naturally leads to a replica prescription in which the geodesic length receives contributions not only from the usual spacetime wormholes of pure JT gravity, but also from replica wormholes associated with the radiation degrees of freedom. These replica wormholes encode the correlations responsible for the Page transition and modify the behaviour of the interior length in an essential way.

For a non-evaporating black hole, the renormalised geodesic length reproduces the expected behaviour: it grows linearly at early times and approaches a plateau at a time exponential in the entropy. In the evaporating case, however, we found a qualitatively different evolution. The ensemble-averaged interior volume initially grows linearly, reaches a maximum close to the Page time, and then decreases exponentially. In this sense, the same non-perturbative gravitational effects that restore

the Page curve for the entropy also leave a sharp imprint on a geometric observable probing the black hole interior.

This behaviour has a natural interpretation from the point of view of subsystem complexity. Before the Page time, the black hole is the larger subsystem and its complexity grows approximately as in the non-evaporating case, although with a rate bounded by the corresponding eternal black hole result. Around the Page time, the black hole and radiation Hilbert spaces become comparable in size. After this point, the black hole subsystem becomes increasingly mixed, and the corresponding subsystem complexity decreases rather than continuing to grow towards the usual complexity plateau.

We also studied the fluctuations of the geodesic length. Before the Page time, the relative fluctuations are parametrically small, so the ensemble average is representative of a typical member of the ensemble. After the Page time, instead, the mean complexity decreases exponentially while the relative fluctuations become large. This signals a loss of self-averaging: the late-time ensemble average is no longer controlled by typical configurations, but is dominated by rare members of the ensemble.

There are several natural directions for future work. One possibility is to extend to the evaporating setup the analysis of geodesic states performed for the non-evaporating black hole [41]. In particular, it would be interesting to study their over-completeness and inner products, since these quantities should now contain additional information associated with the EoW-brane flavour degrees of freedom and with their evolution during evaporation. Another useful diagnostic would be the wormhole velocity for individual members of the ensemble, rather than only after ensemble averaging. This may provide a more refined probe of the interior geometry and could help clarify the relation between complexity growth, rare configurations, and possible firewall-like behaviour [41–43].

It would also be valuable to connect the gravitational calculation presented here more directly with quantum-information models of black hole evaporation. The appearance of combinatorial sums over weighted partitions which play a central role in our computation suggests a universal origin of the result. In view of the correspondence between black holes and random quantum circuits [44, 45], one could ask whether a suitable random circuit model, potentially selected among the proposals of [46–48], reproduces the same pattern found here: early-time growth, a maximum near the Page time, and a smooth post-Page decrease of subsystem complexity. Such a comparison would help determine which aspects of our result are universal features of evaporating chaotic systems and which depend on the specific JT gravity plus EoW-brane ensemble considered in this work.

Acknowledgments

The authors would like to thank Tim Hollowood, Carlos Núñez, Chanju Park and Andrea Legramandi for discussions. SPK would like to acknowledge support from STFC Consolidated Grant Award ST/X000648/1. NB is supported by the STFC DTP grant reference no. ST/Y509644/1.

Open Access Statement - For the purpose of open access, the authors have applied a Creative Commons Attribution (CC BY) licence to any Author Accepted Manuscript version arising.

Data access statement: no new data were generated for this work.

A Genus expansion of pure JT gravity

Pure JT gravity action (2.2) can be re-written as

$$I_{\text{JT}} = -S_0\chi(\mathcal{M}) - \int_{\mathcal{M}} \sqrt{g}\phi(R+2) - 2 \int_{\partial\mathcal{M}} \sqrt{h}\phi(K-1), \quad (\text{A.1})$$

where the first term proportional to S_0 is purely topological and represents the Euler characteristic $\chi = 2 - 2g - n$ of the Riemann surface \mathcal{M} , with g the number of genus and n the number of boundaries of \mathcal{M} . In particular, each time we add a handle to the Euclidean geometry, we increase the genus g of the surface. These handles are often called spacetime wormholes¹⁵ in this context.

The topological term allows us to represent the full path integral as a genus expansion¹⁶

$$\langle Z(\beta_1) \cdots Z(\beta_n) \rangle_C = \sum_{g=0}^{\infty} e^{(2-2g-n)S_0} Z_{g,n}(\beta_1, \dots, \beta_n), \quad (\text{A.2})$$

where $Z_{g,n}$ denotes the contribution from geometries with fixed topology, specifically with g handles.

Exploiting the fact that in a hyperbolic geometry we can always find geodesics homologous to each holographic (or Schwarzian) boundary, we can decompose each surface, associated to $Z_{g,n}$, in a inner hyperbolic surface $\mathcal{M}_{g,n}(\vec{b})$ of genus g bounded by n geodesics of lengths b_i and n trumpets, each describing a hyperbolic space bounded by an holographic boundary of renormalised length β_i and a geodesic of length b_i .

Using this decomposition, it has been found [24]

$$Z_{g,n}(\beta_1, \dots, \beta_n) = \int_0^\infty \left[\prod_{i=1}^n b_i db_i Z_T(\beta_i, b_i) \right] V_{g,n}(b_1, \dots, b_n), \quad (\text{A.3})$$

where $V_{g,n}(b_1, \dots, b_n) = \text{Vol}(\mathcal{M}_{g,n}(\vec{b}))$ is the volume of the interior moduli space, which turn out to be induced by the Weil-Petersson symplectic form, and the integral is over the lengths of the geodesics homologous to each boundary. The remaining factors account for the partition function of the n trumpets geometries, which is one-loop exact and given explicitly by,

$$Z_T(\beta, b) = \frac{e^{-\frac{b^2}{2\beta}}}{\sqrt{2\pi\beta}}. \quad (\text{A.4})$$

¹⁵The reason of this nomenclature is to distinguish them from purely spatial wormholes that live at a fixed time-slice, such as the Einstein-Rosen bridge of an eternal black hole.

¹⁶Multi-boundary correlators need to be computed by summing over all hyperbolic geometries ending on the union of all boundaries, and they can be either connected or disconnected. Whenever we put the subscript C , we are referring to the connected contributions.

The additional b_i factors are due to integral over the moduli τ_i , accounting for a possible twist occurring when the inner geodesic bounded geometry $\mathcal{M}_{g,n}(\vec{b})$ gets glued to the n trumpets.

For the case $n = 2$, the full genus expansion over connected contributions is not fully captured by (A.2), since the double trumpet, i.e. the topologically connected hyperbolic geometry with $n = 2$ and $g = 0$, must be treated separately, and it turns out that,

$$Z_{0,2}(\beta_1, \beta_2) = \int_0^\infty b db Z_T(\beta_1, b) Z_T(\beta_2, b) = \frac{1}{2\pi} \frac{\sqrt{\beta_1 \beta_2}}{\beta_1 + \beta_2}. \quad (\text{A.5})$$

Putting the ingredients together and performing an analytic continuation, one can derive the following key result for the spectral form factor,

$$\langle Z(\beta + it) Z(\beta - it) \rangle = \int dE_1 dE_2 e^{-\beta(E_1 + E_2)} e^{-it(E_1 - E_2)} \langle \rho(E_1) \rho(E_2) \rangle. \quad (\text{A.6})$$

At late times, the integral is dominated by the coincident limit $E_1 \rightarrow E_2$ of the density-density correlator $\langle \rho(E_1) \rho(E_2) \rangle$. At large e^{S_0} and sufficiently away from the spectral edges, it has the following universal form for all matrix integrals with single-cut saddle points [24],

$$\begin{aligned} \langle \rho(E_1) \rho(E_2) \rangle = & \quad (\text{A.7}) \\ e^{2S_0} \rho_D(E_1) \rho_D(E_2) + e^{S_0} \rho_D(E_2) \delta(E_1 - E_2) - & \frac{\sin^2(\pi e^{S_0} \rho_D(E_2)(E_1 - E_2))}{\pi^2 (E_1 - E_2)^2}. \end{aligned}$$

B Partition function JT gravity with EoW brane

The fully connected disc partition function for JT gravity with n AdS boundaries and n EoW branes is,

$$Z_n = e^{S_0} \int ds \rho_D(s) y(s)^n, \quad (\text{B.1})$$

with

$$\rho_D(s) = \frac{s}{2\pi^2} \sinh(2\pi s), \quad y(s) = e^{-\frac{\beta s^2}{2}} \left| \Gamma\left(\mu + \frac{1}{2} + is\right) \right|^2. \quad (\text{B.2})$$

The semiclassical limit is $\beta \ll 1$ corresponding to high temperatures. Upon restoring Newton's constant, it is equivalent to the $G_N \rightarrow 0$ limit.

For large brane tension $\mu \rightarrow \infty$, or more precisely $\mu \gg 1/\beta$ (the partition function at high temperatures will only have support near $s \approx 2\pi/n\beta$), the product of Gamma functions is well approximated using Stirling's formula as a μ -dependent constant,

$$y(s) \approx e^{-\frac{\beta s^2}{2}} \mu^{2\mu}. \quad (\text{B.3})$$

Therefore to get the small- β saddle point, we use

$$\rho(s) y(s)^n \approx \frac{s}{4\pi^2} y(0)^n e^{2\pi s - n\beta s^2/2}, \quad (\text{B.4})$$

from which we get the saddle point value of s

$$s_{\mu \gg 1}^{(n)} = \frac{2\pi}{n\beta} + \mathcal{O}(1). \quad (\text{B.5})$$

Therefore, in the large brane tension limit, Z_n is proportional to the thermal partition function of pure JT gravity at inverse temperature $n\beta$, and with a classical geometry given by the disc of boundary length $n\beta$.

In the tensionless brane limit, on the other hand,

$$y(s) = e^{-\frac{\beta s^2}{2}} \frac{\pi}{\cosh \pi s} \approx 2\pi e^{-\pi s - \frac{\beta s^2}{2}}, \quad (\text{B.6})$$

and

$$\rho(s) y(s)^n \approx \frac{s}{\pi} e^{(2-n)\pi s - n\beta s^2/2}, \quad (\text{B.7})$$

with saddle point when $n < 2$,

$$s_{\mu \ll 1}^{(n)} = \frac{(2-n)\pi}{n\beta} + \mathcal{O}(1). \quad (\text{B.8})$$

Thus only Z_1 has a classical (real) saddle which is a half disc. This means that the effective temperature is $\frac{1}{2\beta}$ and the classical geometry can be thought of as a \mathbb{Z}_2 quotient of the thermal disc.

C Review of complexity computation in JT with EoW brane

In this section we review the calculation of the non-perturbative geodesic length for JT gravity with an EoW brane (without attached degrees of freedom) carried out in [11] following on from the original work without EoW branes [12]. Let us start by writing the two-point function¹⁷ at disc level,

$$\begin{aligned} \langle \mathcal{O}_1(u) \mathcal{O}_2(0) \rangle_D &= \frac{1}{Z_{D,\mu}(\beta)} \int_0^\infty \frac{dz}{z} \Psi_D(\beta - u, L) \Psi_D(u, L) \left(\frac{z}{4}\right)^\Delta \\ &= \frac{2e^{S_0}}{Z_{D,\mu}(\beta)} \int_0^\infty dE_1 dE_2 e^{-(\beta-u)E_1 - uE_2} \gamma_\mu(E_1) \gamma_\mu(E_2) \rho_D(E_1) \rho_D(E_2) \mathcal{M}_\Delta(E_1, E_2), \end{aligned} \quad (\text{C.1})$$

¹⁷In this section, by two-point function we mean a correlation function between two operators, one located at the asymptotic boundary and the other on the EoW brane.

where we have defined

$$\mathcal{M}_\Delta(E_1, E_2) = \int_0^\infty \frac{dz}{z^2} W_{-\mu, i\sqrt{2E_1}}(z) W_{-\mu, i\sqrt{2E_2}}(z) \left(\frac{z}{4}\right)^\Delta, \quad z = 4e^{-L}. \quad (\text{C.2})$$

The disc-level two-point function (C.1) can be obtained by using the boundary particle formalism introduced in [30], according to which the full quantum gravity two-point function can be obtained by dressing the CFT two-point function $e^{-\Delta L} = (z/4)^\Delta$ with an appropriate kernel which, in this case, is the Hartle-Hawking wavefunction (4.10).

Higher genus and nonperturbative contributions can be included by performing the following substitution,

$$e^{2S_0} \rho_D(E_1) \rho_D(E_2) \rightarrow \langle \rho(E_1) \rho(E_2) \rangle, \quad (\text{C.3})$$

i.e. by replacing the leading disc contribution of the two-point correlation of the spectral density with its full nonperturbative expression (A.7). The extension, natural from a random matrix point of view, has been proven in [12] to yield the full two-point function at any genus, evaluated on any non self-intersecting geodesics connecting the two insertions.

Now we may analytically continue u to real time,

$$u \rightarrow \frac{\beta}{2} + it, \quad (\text{C.4})$$

and extract the geodesic length from the full two-point function via,

$$\langle L(t) \rangle = - \lim_{\Delta \rightarrow 0} \frac{\partial \langle O\left(\frac{\beta}{2} + it\right) O(0) \rangle}{\partial \Delta}. \quad (\text{C.5})$$

All dependence of the two-point function on Δ resides in $\mathcal{M}_\Delta(E_1, E_2)$, so we can differentiate with respect to Δ inside the energy integral. Then, using “center of mass” and relative variables,

$$E = \frac{E_1 + E_2}{2}, \quad \omega = E_1 - E_2, \quad dE_1 dE_2 = dE d\omega, \quad (\text{C.6})$$

we find, using known integrals involving Whittaker functions [49],

$$\lim_{\Delta \rightarrow 0} \frac{\partial \mathcal{M}_\Delta(E_1, E_2)}{\partial \Delta} = \frac{\sqrt{2E}}{2\pi \gamma_\mu(E) \rho_D(E)} \frac{1}{\omega^2} + \mathcal{O}(\omega^{-1}). \quad (\text{C.7})$$

Combining all, we get,

$$\langle L(t) \rangle = L_{\text{div}} - \frac{e^{S_0}}{\pi Z_{D,\mu}(\beta)} \int_0^\infty dE e^{-\beta E} \sqrt{2E} \gamma_\mu(E) \rho_D(E) \times \quad (\text{C.8})$$

$$\times \int_{-\infty}^\infty d\omega \left(1 - \frac{\sin^2(\pi \rho_D(E) e^{S_0} \omega)}{(\pi \rho_D(E) e^{S_0} \omega)^2} \right) e^{i\omega t} \left(\frac{1}{\omega^2} + \mathcal{O}(\omega^{-1}) \right). \quad (\text{C.9})$$

The contact term in (A.7) leads to a divergent and t -independent contribution, while the inclusion of subleading terms of order $\mathcal{O}(\omega^{-1})$ on the right hand side above, leads to similar or vanishing contributions.

As emphasized in [12], the renormalization prescription for the length operator is to consider the quantity $\langle L(t) - L(0) \rangle$, which is free of divergences and independent of regularisation scheme. Importantly, the renormalised length captures the expected late time physics of complexity evolution.

The final frequency integral in (C.9) can be evaluated exactly. The integrand is regular at $\omega = 0$, due to the cancellation between the semi-classical disconnected piece and the non-perturbative contributions. However, we can evaluate it by expanding the sine in terms of complex exponentials and evaluating each contribution by contour integration, avoiding the putative pole in each term at $\omega = 0$. The ω -integral is then performed by closing the contour in the upper half-plane for $t > \pi\rho_D(E)e^{S_0}$, when the integral vanishes, since the contour does not enclose any poles. On the other hand, for $0 < t < \pi\hat{\rho}_D(E)e^{S_0}$, we find a non-zero residue,

$$\int_{-\infty}^{\infty} d\omega \frac{e^{i\omega t}}{\omega^2} \left(1 - \frac{\sin^2(\alpha_D\omega)}{(\alpha_D\omega)^2} \right) = \frac{2\pi\alpha_D}{3} \left(1 - \frac{t}{2\alpha_D} \right)^3, \quad (\text{C.10})$$

where $\alpha_D(E) = \pi\rho_D(E)e^{S_0}$. Therefore, we finally obtain,

$$\langle L(t) \rangle = L_{\text{div}} - \frac{2\pi e^{2S_0}}{3Z_{D,\mu}(\beta)} \int_{E_*}^{\infty} dE e^{-\beta E} \sqrt{2E} \gamma_{\mu}(E) \rho_D^2(E) \left(1 - \frac{t}{2\alpha(E)} \right)^3. \quad (\text{C.11})$$

where E_* is implicitly obtained via the equation $2\pi\rho_D(E_*)e^{S_0} = t$. Then the renormalised length or complexity exhibits linear growth, saturating at late times,

$$\mathcal{C}(t) = \langle L(t) - L(0) \rangle \approx \begin{cases} c_1 t + \dots & t \ll e^{S_0}, \\ c_0 - \dots & t \gg e^{S_0}, \end{cases} \quad (\text{C.12})$$

where $c_0 \sim e^{S_0}$ and $c_1 \simeq \frac{2\pi}{\beta}$ in the semiclassical and large brane tension limit. The linear growth followed by a plateau, at a value and time exponential in the entropy of the black hole, is consistent with Susskind's conjecture [14–17].

D Page curve

The fine-grained entanglement entropy of Hawking radiation can be extracted using the replica trick via

$$S_R = \lim_{n \rightarrow 1} \frac{1}{1-n} \log(\text{Tr}(\rho_R^n)) = - \lim_{n \rightarrow 1} \frac{\partial}{\partial n} \log(\text{Tr}(\rho_R^n)) = - \lim_{n \rightarrow 1} \frac{\partial}{\partial n} \text{Tr}(\rho_R^n), \quad (\text{D.1})$$

where

$$\mathrm{Tr}(\rho_R^n) = \frac{\overline{Z^n}}{(kZ_1)^n}. \quad (\text{D.2})$$

In the planar limit, we can compute $\overline{Z^n}$ by considering all possible ways of filling in the bulk n boundary conditions as the one pictured in Figure 3, neglecting both handles and brane crossing as explained in the main text.

It turns out that

$$(\overline{Z^n})_{\text{planar}} = k \sum_{j=1}^n \sum_{\substack{r_1, \dots, r_n \geq 0 \\ \sum_{m=1}^n m r_m = n \\ \sum_{m=1}^n r_m = j}} \frac{n!}{(n-j+1)! \prod_{m=1}^n r_m!} \prod_{m=1}^n (k^{m-1} Z_m(\beta))^{r_m}, \quad (\text{D.3})$$

where r_m is the number of connected geometries with m replica boundaries, yielding a total of $1 \leq j \leq n$ connected blocks constructed out of n pairs of asymptotic boundary/EoW brane.

The above complicate expression gets considerably simplified in the microcanonical ensemble, since we need to perform the following replacement

$$Z_m \rightarrow \mathbf{Z}_m = e^{\mathbf{S}} y(E)^m, \quad (\text{D.4})$$

and (D.3) becomes

$$(\overline{\mathbf{Z}^n})_{\text{planar}} = y(E)^n \sum_{j=1}^n k^{n-j+1} e^{\mathbf{S}j} \sum_{\substack{r_1, \dots, r_n \geq 0 \\ \sum_{m=1}^n m r_m = n \\ \sum_{m=1}^n r_m = j}} \frac{n!}{(n-j+1)! \prod_{m=1}^n r_m!}. \quad (\text{D.5})$$

Now the last sum in (D.5) gives the so called Narayana numbers $N(n, j)$, counting the *non-crossing*¹⁸ partitions in which a set of n elements is partitioned in exactly j blocks, which get simplified into

$$N(n, j) = \frac{1}{n} \binom{n}{j} \binom{n}{j-1}. \quad (\text{D.6})$$

Therefore the n -Rényi entropy can be written as

$$\mathrm{Tr}(\rho_R^n) = \sum_{j=1}^n N(n, j) k^{j-n} e^{\mathbf{S}(1-j)} = \sum_{j=1}^n N(n, j) k^{1-j} e^{\mathbf{S}(j-n)}, \quad (\text{D.7})$$

specifically in two equivalent ways, related to the fact that (D.3) is symmetric under the $k \leftrightarrow e^{\mathbf{S}}$ swapping. However, as explained in [50], the two equivalent expressions

¹⁸It is worth remarking that in the replica trick applied to compute the ensemble averaged boundary-brane two-point function we did not consider non-crossing partitions, since there was not a global trace/cycle imposing it, as it is the case for the n -Rényi entropy (D.2).

yield two analytic continuations to real n , each satisfying the Carlson theorem in different and complementary ranges, specifically

$$\text{Tr}(\rho_R^n) = k^{1-n} {}_2F_1\left(1-n, -n; 2; \frac{k}{e^{\mathbf{S}}}\right) \Theta(e^{\mathbf{S}} - k) + q^{1-n} {}_2F_1\left(1-n, -n; 2; \frac{e^{\mathbf{S}}}{k}\right) \Theta(k - e^{\mathbf{S}}). \quad (\text{D.8})$$

Finally we get the entanglement entropy, perfectly consistent with the original result obtained by Page [4],

$$S(R) = \left(\log k - \frac{k}{2e^{\mathbf{S}}}\right) \Theta(e^{\mathbf{S}} - k) + \left(\mathbf{S} - \frac{e^{\mathbf{S}}}{2k}\right) \Theta(k - e^{\mathbf{S}}). \quad (\text{D.9})$$

This derivation of the Page curve has been similarly found in [51, 52].

E More on the complexity computation

E.1 Truncation of $\exp(\#\omega\beta)$ factors in the kernel $\mathcal{I}(n)$

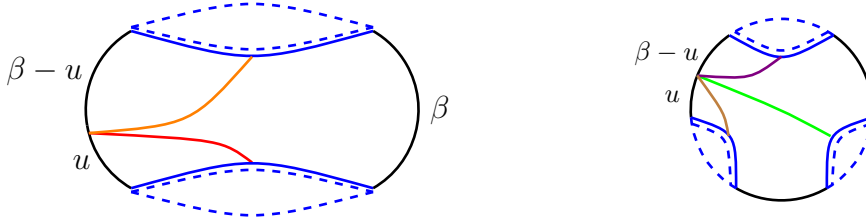


Figure 11: Depiction of all naively inequivalent geodesics stretching between an asymptotic boundary and an EoW brane in a fully connected $n = 2$ (left) and $n = 3$ (right) replica wormhole geometry. The geodesics' colors match the ones of the corresponding Boltzmann weights in eq. (E.1) and eq. (E.2).

If we computed (5.9) keeping the the $e^{\#\omega\beta}$ factors consistently, we would get

$$\begin{aligned} \left\langle \sum_{A=1}^2 O_{1,A} \sum_{B=1}^2 O_{2,B} \right\rangle \overline{Z^2} = & \quad (\text{E.1}) \\ & 2e^{S_0} \int_0^\infty dE d\omega \left\langle \rho\left(E + \frac{\omega}{2}\right) \rho\left(E - \frac{\omega}{2}\right) \right\rangle \gamma_\mu(E) \mathcal{M}_\Delta(E, \omega) \times \\ & \times \left[e^{-\beta E} \gamma_\mu(E) k \cdot 1 \cdot 1 \cdot \binom{2}{1} Z_1 + e^{-2\beta E} \gamma_\mu(E)^2 k^2 \cdot 2 \cdot \left(e^{\frac{\omega\beta}{2}} + e^{-\frac{\omega\beta}{2}} \right) \binom{2}{2} \right], \end{aligned}$$

and similarly, in the $n = 3$ case,

$$\begin{aligned} \left\langle \sum_{A=1}^3 O_{1,A} \sum_{B=1}^3 O_{2,B} \right\rangle \overline{Z^3} &= 2e^{S_0} \int_0^\infty dE d\omega \left\langle \rho \left(E + \frac{\omega}{2} \right) \rho \left(E - \frac{\omega}{2} \right) \right\rangle \times \quad (\text{E.2}) \\ &\gamma_\mu(E) \mathcal{M}_\Delta(E, \omega) \left[e^{-\beta E} \gamma_\mu(E) k \cdot 1 \cdot 1 \cdot \binom{3}{1} (Z_1^2 + k Z_2) + \right. \\ &e^{-2\beta E} \gamma_\mu(E)^2 k^2 \cdot 2 \left(e^{\frac{\omega\beta}{2}} + e^{-\frac{\omega\beta}{2}} \right) \binom{3}{2} Z_1 + \\ &\left. + e^{-3\beta E} \gamma_\mu(E)^3 k^3 \cdot 3 \left(e^{\omega\beta} + e^0 + e^{-\omega\beta} \right) \binom{3}{3} \right]. \end{aligned}$$

Carrying out the prescription for general positive integer n ,

$$\begin{aligned} \mathcal{I}(n) &= \quad (\text{E.3}) \\ &\sum_{j=1}^n (y(E))^j k^j j \sum_{m=0}^{j-1} \left[e^{(\frac{j-1}{2}-m)\omega\beta} \right] \binom{n}{j} B_{n-j}(k^0 Z_1, k^1 Z_2, \dots, k^{n-j-1} Z_{n-j}), \end{aligned}$$

yielding, in the microcanonical ensemble,

$$\left. \frac{\partial \mathcal{I}(n)}{\partial n} \right|_{n=0} = e^{-a} \sum_{r=0}^{\infty} \left[\frac{a^r}{r!} \frac{e^{\frac{\omega\beta}{2} r}}{(e^{\frac{\omega\beta}{2}} + r)(1 + e^{\frac{\omega\beta}{2} r})} \right] = e^{-a} \sum_{r=0}^{\infty} \left[\frac{a^r}{r!} \frac{r}{(1+r)^2} \right] + \mathcal{O}(\omega^2). \quad (\text{E.4})$$

Similarly, in the canonical ensemble $\mathcal{I}'(0)$ (E.17) acquires $\mathcal{O}(\omega^2)$ corrections.

Therefore, our truncation

$$\sum_{m=0}^{j-1} \left[e^{(\frac{j-1}{2}-m)\omega\beta} \right] \simeq j, \quad (\text{E.5})$$

is well justified.

E.2 Computation of $\mathcal{I}(n)$ in the canonical ensemble

Using the rescaled variables (7.1), (7.2) and the isobaric property of the complete Bell polynomials we re-express (5.21) in a more malleable form:

$$\mathcal{I}(n) = k^n \sum_{p=1}^n y(s)^p p^2 \binom{n}{p} B_{n-p}(a_0 \hat{Z}_1, a_0 \hat{Z}_2, \dots, a_0 \hat{Z}_{n-p}). \quad (\text{E.6})$$

Given the generating function $B(z)$ for the complete Bell polynomials (7.4), let us also define the series

$$A(z) \equiv \sum_{p=1}^{\infty} y(s)^p p^2 \frac{z^p}{p!} = e^{y(s)z} y(s)z (1 + y(s)z). \quad (\text{E.7})$$

Exploiting the convolution property of two power series, according to which, given two power series

$$A(z) = \sum_{m=0}^{\infty} \mathcal{A}_m \frac{z^m}{m!}, \quad B(z) = \sum_{m=0}^{\infty} \mathcal{B}_m \frac{z^m}{m!}, \quad (\text{E.8})$$

the product $C(z) = A(z)B(z)$ is a power series given by

$$C(z) = \sum_{n=0}^{+\infty} \mathcal{C}_n \frac{z^n}{n!}, \quad \mathcal{C}_n = \sum_{j=0}^n \binom{n}{j} \mathcal{A}_j \mathcal{B}_{n-j}, \quad (\text{E.9})$$

we can easily observe that $\mathcal{I}(n)$ (5.21) can be expressed as

$$\mathcal{I}(n) = k^n n! [z^n] A(z) B(z), \quad (\text{E.10})$$

where $[\dots]$ denotes ‘‘coefficient of \dots ’’. $B(z)$ in (7.4) has a compact form,

$$B(z) = e^{-a_0 M} \exp \left[a_0 \int_0^{\infty} ds' \rho(s') e^{y(s')z} \right] \quad (\text{E.11})$$

$$= e^{-a_0 M} \sum_{r=0}^{\infty} \left[\frac{a_0^r}{r!} \int_0^{+\infty} \prod_{k=1}^r (ds_k \rho(s_k)) e^{S_r z} \right], \quad (\text{E.12})$$

where we used (5.1) in the first equality, and defined

$$M \equiv \int_0^{\infty} ds' \rho(s'), \quad S_r \equiv \sum_{k=1}^r y(s_k). \quad (\text{E.13})$$

Then (E.10) becomes

$$\mathcal{I}(n) = e^{-a_0 M} \sum_{r=0}^{\infty} \left[\frac{a_0^r}{r!} \int_0^{+\infty} \prod_{k=1}^r (ds_k \rho(s_k)) (k^n n! [z^n] A(z) e^{S_r z}) \right]. \quad (\text{E.14})$$

Applying once again the series convolution property (E.9),

$$n! [z^n] A(z) e^{S_r z} = \sum_{j=0}^n \mathcal{A}_j S_r^{n-j} \binom{n}{j} \quad (\text{E.15})$$

$$= n S_r^{n-1} y(s) \left(1 + \frac{y(s)}{S_r} \right)^{n-2} \left(1 + n \frac{y(s)}{S_r} \right), \quad (\text{E.16})$$

we finally take the derivative with respect to n and send $n \rightarrow 0$, obtaining the intermediate result,

$$\mathcal{I}'(0) \equiv \left. \frac{\partial \mathcal{I}(n)}{\partial n} \right|_{n=0} = e^{-a_0 M} y(s) \sum_{r=0}^{+\infty} \left[\frac{a_0^r}{r!} \int_0^{+\infty} \prod_{k=1}^r (ds_k \rho(s_k)) \frac{S_r}{(S_r + y(s))^2} \right]. \quad (\text{E.17})$$

At this point, we note that the last factor of the integrand can be written as a Laplace transform

$$\frac{S_r}{(S_r + y(s))^2} = \int_0^{+\infty} d\chi \chi e^{-\chi(S_r + y(s))} S_r, \quad (\text{E.18})$$

so that (E.17) becomes

$$\mathcal{I}'(0) = e^{-a_0 M} y(s) \sum_{r=0}^{+\infty} \left[\frac{a_0^r}{r!} \int_0^{+\infty} d\chi \chi e^{-\chi y(s)} \times \right. \quad (\text{E.19})$$

$$\left. \times \left(\sum_{j=1}^r \int_0^{+\infty} ds_j \rho(s_j) y(s_j) e^{-\chi y(s_j)} \right) \left(\prod_{k \neq j} \int_0^{+\infty} ds_k \rho(s_k) e^{-\chi y(s_k)} \right) \right], \quad (\text{E.20})$$

or more compactly

$$\mathcal{I}'(0) = e^{-a_0 M} y(s) \int_0^{+\infty} d\chi (\chi e^{-\chi y(s)}) \left[\sum_{r=0}^{+\infty} r \frac{a_0^r}{r!} I_1(\chi) I_0(\chi)^{r-1} \right], \quad (\text{E.21})$$

where we introduced the following notation

$$I_0(\chi) = \int_0^{+\infty} ds \rho(s) e^{-\chi y(s)}, \quad (\text{E.22})$$

$$I_1(\chi) = \int_0^{+\infty} ds \rho(s) y(s) e^{-\chi y(s)}. \quad (\text{E.23})$$

Performing the r -series in (E.21), we get

$$\begin{aligned} \mathcal{I}'(0) &= e^{-a_0 M} a y(s) \int_0^{+\infty} d\chi (\chi e^{-\chi y(s)}) I_1(\chi) e^{a_0 I_0(\chi)} \quad (\text{E.24}) \\ &= y(s) \int_0^{+\infty} d\chi (1 - \chi y(s)) e^{-\chi y(s)} \exp \left[a_0 \int_0^{+\infty} ds'' \rho(s'') (e^{-\chi y(s'')} - 1) \right], \end{aligned}$$

where to get to the last step we performed an integration by parts recognising,

$$\begin{aligned} &- a_0 \left(\int_0^{+\infty} ds' \rho(s') y(s') e^{-\chi y(s')} \right) \exp \left[a_0 \int_0^{+\infty} ds'' \rho(s'') (e^{-\chi y(s'')} - 1) \right] \\ &= \partial_\chi \left(\exp \left[a_0 \int_0^{+\infty} ds'' \rho(s'') (e^{-\chi y(s'')} - 1) \right] \right). \quad (\text{E.25}) \end{aligned}$$

Furthermore, let us note that if we go to the microcanonical ensemble, we get exactly (6.8), which represents a strong consistency check that the correct analytic continuation in n has been carried out.

E.3 Leading contribution of the canonical ensemble computation

In this subsection we are going to derive the leading contribution of the complexity evolution in the canonical ensemble for arbitrary time.

First of all, let us notice that the integral (7.10) can be analytically solvable in the following two regimes

$$\Phi(u) \simeq \begin{cases} \frac{u}{\sqrt{2\pi}\beta^{3/2}} e^{\frac{2\pi^2}{\beta}} & u \ll e^{\frac{2\pi^2}{\beta}}, \\ \frac{1}{(2\pi)^3} e^{2\pi\sqrt{\frac{2}{\beta}\log(u)}} \sqrt{\frac{2}{\beta}\log(u)} & u \gg e^{\frac{2\pi^2}{\beta}}. \end{cases} \quad (\text{E.26})$$

In the follow, we are going to prove that the kernel integral $\mathcal{I}'(0)$ (7.9), in the regime $u \leq u_{<} \ll e^{\frac{2\pi^2}{\beta}}$, turns out to give the main contribution to the complexity.

In the latter u -range, we get straightforwardly

$$\mathcal{I}'(0)_{\text{main}} = \hat{y}(s) \frac{e^{-u_{<}(\hat{y}(s)+a_0\hat{Z}(\beta))} \left[a_0\hat{Z}(\beta) \left(-1 + e^{u_{<}(\hat{y}(s)+a_0\hat{Z}(\beta))} \right) + u_{<}\hat{y}(s) \left(\hat{y}(s) + a_0\hat{Z}(\beta) \right) \right]}{\left(\hat{y}(s) + a_0\hat{Z}(\beta) \right)^2}, \quad (\text{E.27})$$

where

$$\hat{Z}(\beta) = \frac{e^{\frac{2\pi^2}{\beta}}}{\sqrt{2\pi}\beta^{3/2}}, \quad (\text{E.28})$$

is the (un-normalized) disc-partition function evaluated in the saddle-point approximation. Plugging the kernel contribution (E.27) into eq. (7.7) yields, upon performing a saddle-point approximation,

$$\mathcal{C}(t)_{\text{main}} \simeq a_0 t \sqrt{2\pi} \frac{e^{\frac{4\pi^2}{\beta}} a_0 \hat{Z}(\beta) e^{\frac{2\pi^2}{\beta}} + e^{-a_0 \hat{Z}(\beta) e^{\frac{2\pi^2}{\beta}}} \beta \left(-a_0 \hat{Z}(\beta) + \beta e^{-\frac{2\pi^2}{\beta}} \right)}{\beta^{5/2} \left(1 + a_0 \hat{Z}(\beta) e^{\frac{2\pi^2}{\beta}} \right)^2}, \quad (\text{E.29})$$

where we chose $u_{<} = e^{\frac{2\pi^2}{\beta}} \beta \ll e^{\frac{2\pi^2}{\beta}}$.

Regarding the u -tail, let us notice that

$$\mathcal{I}'(0)_{\text{tail}} = \int_{u_{>}}^{+\infty} du (1 - u\hat{y}(s)) e^{-u\hat{y}(s)} e^{-a_0\Phi_{\text{tail}}(u)}, \quad (\text{E.30})$$

is dominated around the lower endpoint $u = u_{>} \gg e^{\frac{2\pi^2}{\beta}}$. Therefore, using the Laplace endpoint approximation, the above integral reduces to

$$\mathcal{I}'(0)_{\text{tail}} \simeq \frac{\hat{y}(s)(1 - u_{>}\hat{y}(s))}{(a_0\Phi'_{\text{tail}}(u_{>}) + \hat{y}(s))} e^{-u_{>}\hat{y}(s) - a_0\Phi_{\text{tail}}(u_{>})}, \quad (\text{E.31})$$

which, upon taking $u_{>} = \beta^{-1} e^{\frac{2\pi^2}{\beta}} \gg e^{\frac{2\pi^2}{\beta}}$ and performing the saddle point approximation, yields the following complexity tail contribution

$$\mathcal{C}(t)_{\text{tail}} \simeq -a_0 t \sqrt{2\pi} \frac{e^{\frac{4\pi^2}{\beta}}}{\beta^{5/2}} \frac{e^{-\frac{1}{\beta} - (2\pi)^{3/2} \beta^{1/2} a_0 \hat{Z}(\beta) e^{\frac{2\pi^2}{\beta}}}}{\beta \left(1 + (2\pi\beta)^{3/2} a_0 \hat{Z}(\beta) e^{\frac{2\pi^2}{\beta}}\right)}. \quad (\text{E.32})$$

The complexity contribution due to the gap region $u_{<} < u < u_{>}$ can be computed by using the following uniform approximation for $\Phi(u)$,

$$\Phi(u) = \int_0^{s_*} ds \rho(s) + u \int_{s_*}^{+\infty} ds \rho(s) \hat{y}(s), \quad (\text{E.33})$$

where, in the gap region,

$$s_* = \sqrt{\frac{2}{\beta} \log u} \simeq \frac{2\pi}{\beta} + \mathcal{O}(\beta \log \beta). \quad (\text{E.34})$$

Finally, one finds at leading order,

$$\mathcal{C}(t)_{\text{gap}} \simeq a_0 t \sqrt{2\pi} \frac{e^{\frac{4\pi^2}{\beta}}}{\beta^{5/2}} \frac{(a_0 \hat{Z}(\beta) + e^{-\frac{2\pi^2}{\beta}}) e^{-\frac{1}{\beta} (a_0 \hat{Z}(\beta) e^{\frac{2\pi^2}{\beta}} + 1)}}{\beta \left(1 + a_0 \hat{Z}(\beta) e^{\frac{2\pi^2}{\beta}}\right)^2}. \quad (\text{E.35})$$

It is straightforward to check that the leading-order contribution at all times is due to $\mathcal{C}(t)_{\text{main}}$ (E.29), explicitly

$$\boxed{\mathcal{C}(t) \simeq t \sqrt{2\pi} \frac{e^{\frac{4\pi^2}{\beta}}}{\beta^{5/2}} \frac{a_0^2 \hat{Z}(\beta) e^{\frac{2\pi^2}{\beta}}}{\left(1 + a_0 \hat{Z}(\beta) e^{\frac{2\pi^2}{\beta}}\right)^2} = \frac{2\pi}{\beta} t \frac{e^{2(s_0 + \frac{4\pi^2}{\beta})}}{\left(\sqrt{2\pi} \beta^{3/2} k + e^{s_0 + \frac{4\pi^2}{\beta}}\right)^2}}. \quad (\text{E.36})$$

One can argue that, at zero-th order in the $a_0 \rightarrow 0$ limit, eq. (E.36) does not capture a residual non-vanishing complexity displayed by both the tail and the gap contributions. However, this limit can be studied exactly through

$$\mathcal{I}'(0) = \hat{y}(s) \int_0^{+\infty} du (1 - u \hat{y}(s)) e^{-u \hat{y}(s)} = 0, \quad (\text{E.37})$$

leading us to conclude that eq. (E.36) captures all the complexity behaviour in the canonical ensemble.

References

- [1] S. W. Hawking, “Particle Creation by Black Holes,” *Commun. Math. Phys.* **43** (1975), 199-220
- [2] S. W. Hawking, “Breakdown of Predictability in Gravitational Collapse,” *Phys. Rev. D* **14**, 2460-2473 (1976)
- [3] D. N. Page, “Information in black hole radiation,” *Phys. Rev. Lett.* **71**, 3743-3746 (1993) [[arXiv:hep-th/9306083](#) [hep-th]].
- [4] D. N. Page, “Average entropy of a subsystem,” *Phys. Rev. Lett.* **71**, 1291-1294 (1993) [[arXiv:gr-qc/9305007](#) [gr-qc]].
- [5] G. Penington, “Entanglement Wedge Reconstruction and the Information Paradox,” *JHEP* **09**, 002 (2020) [[arXiv:1905.08255](#) [hep-th]].
- [6] G. Penington, S. H. Shenker, D. Stanford and Z. Yang, “Replica wormholes and the black hole interior,” *JHEP* **03**, 205 (2022) [[arXiv:1911.11977](#) [hep-th]].
- [7] A. Almheiri, T. Hartman, J. Maldacena, E. Shaghoulian and A. Tajdini, “Replica Wormholes and the Entropy of Hawking Radiation,” *JHEP* **05** (2020), 013 [[arXiv:1911.12333](#) [hep-th]].
- [8] C. Teitelboim, “Gravitation and Hamiltonian Structure in Two Space-Time Dimensions,” *Phys. Lett. B* **126** (1983), 41-45
- [9] R. Jackiw, “Lower Dimensional Gravity,” *Nucl. Phys. B* **252** (1985), 343-356
- [10] J. Maldacena, D. Stanford and Z. Yang, “Conformal symmetry and its breaking in two dimensional Nearly Anti-de-Sitter space,” *PTEP* **2016** (2016) no.12, 12C104 [[arXiv:1606.01857](#) [hep-th]].
- [11] M. Alishahiha, S. Banerjee and J. Kames-King, “Complexity via replica trick,” *JHEP* **08** (2022), 181 doi:10.1007/JHEP08(2022)181 [[arXiv:2205.01150](#) [hep-th]].
- [12] L. V. Iliesiu, M. Mezei and G. Sárosi, “The volume of the black hole interior at late times,” *JHEP* **07** (2022), 073 doi:10.1007/JHEP07(2022)073 [[arXiv:2107.06286](#) [hep-th]].
- [13] L. Susskind, “Computational Complexity and Black Hole Horizons,” *Fortsch. Phys.* **64** (2016), 24-43 [[arXiv:1403.5695](#) [hep-th]].
- [14] L. Susskind, “The Typical-State Paradox: Diagnosing Horizons with Complexity,” *Fortsch. Phys.* **64** (2016), 84-91 [[arXiv:1507.02287](#) [hep-th]].
- [15] A. R. Brown, L. Susskind and Y. Zhao, “Quantum Complexity and Negative Curvature,” *Phys. Rev. D* **95** (2017) no.4, 045010 [[arXiv:1608.02612](#) [hep-th]].
- [16] L. Susskind, “Black Holes at Exp-time,” [[arXiv:2006.01280](#) [hep-th]].
- [17] V. Balasubramanian, M. Decross, A. Kar and O. Parrikar, “Quantum Complexity of Time Evolution with Chaotic Hamiltonians,” *JHEP* **01** (2020), 134 [[arXiv:1905.05765](#) [hep-th]].

- [18] M. Alishahiha, “Holographic Complexity,” *Phys. Rev. D* **92** (2015) no.12, 126009 [[arXiv:1509.06614](#) [hep-th]].
- [19] B. Chen, W. M. Li, R. Q. Yang, C. Y. Zhang and S. J. Zhang, “Holographic subregion complexity under a thermal quench,” *JHEP* **07** (2018), 034 [[arXiv:1803.06680](#) [hep-th]].
- [20] C. A. Agón, M. Headrick and B. Swingle, “Subsystem Complexity and Holography,” *JHEP* **02** (2019), 145 [[arXiv:1804.01561](#) [hep-th]].
- [21] D. Carmi, R. C. Myers and P. Rath, “Comments on Holographic Complexity,” *JHEP* **03** (2017), 118 [[arXiv:1612.00433](#) [hep-th]].
- [22] O. Aharony and V. Narovlansky, “Renormalization group flow in field theories with quenched disorder,” *Phys. Rev. D* **98** (2018) no.4, 045012 [[arXiv:1803.08534](#) [hep-th]].
- [23] N. Engelhardt, S. Fischetti and A. Maloney, “Free energy from replica wormholes,” *Phys. Rev. D* **103** (2021) no.4, 046021 [[arXiv:2007.07444](#) [hep-th]].
- [24] P. Saad, S. H. Shenker and D. Stanford, “JT gravity as a matrix integral,” [[arXiv:1903.11115](#) [hep-th]].
- [25] P. Saad, “Late Time Correlation Functions, Baby Universes, and ETH in JT Gravity,” [[arXiv:1910.10311](#) [hep-th]].
- [26] A. Blommaert, “Dissecting the ensemble in JT gravity,” *JHEP* **09** (2022), 075 [[arXiv:2006.13971](#) [hep-th]].
- [27] I. Kourkoulou and J. Maldacena, “Pure states in the SYK model and nearly- AdS_2 gravity,” [[arXiv:1707.02325](#) [hep-th]].
- [28] P. Gao, D. L. Jafferis and D. K. Kolchmeyer, “An effective matrix model for dynamical end of the world branes in Jackiw-Teitelboim gravity,” *JHEP* **01** (2022), 038 [[arXiv:2104.01184](#) [hep-th]].
- [29] D. Harlow and D. Jafferis, “The Factorization Problem in Jackiw-Teitelboim Gravity,” *JHEP* **02** (2020), 177 [[arXiv:1804.01081](#) [hep-th]].
- [30] Z. Yang, “The Quantum Gravity Dynamics of Near Extremal Black Holes,” *JHEP* **05** (2019), 205 [[arXiv:1809.08647](#) [hep-th]].
- [31] D. Stanford and E. Witten, “Fermionic Localization of the Schwarzian Theory,” *JHEP* **10** (2017), 008 [[arXiv:1703.04612](#) [hep-th]].
- [32] A. Kitaev and S. J. Suh, “Statistical mechanics of a two-dimensional black hole,” *JHEP* **05** (2019), 198 [[arXiv:1808.07032](#) [hep-th]].
- [33] N. Iizuka and M. Nishida, “A note on the non-planar corrections for the Page curve in the PSSY model via the IOP matrix model correspondence,” *JHEP* **12** (2025), 212 [[arXiv:2410.04679](#) [hep-th]].
- [34] E. T. Bell, “Exponential Polynomials,” *Annals of Mathematics* **35** (2): 258–277, (1934).

- [35] L. Comtet, “Advanced Combinatorics The Art of Finite and Infinite Expansions,” D. Reidel Publishing Company, Dordrecht, (1974).
- [36] R. B. Paris, “The asymptotics of the Touchard polynomials”, [arXiv:1606.07883](#) [math.CA].
- [37] D. Marolf and H. Maxfield, “Transcending the ensemble: baby universes, spacetime wormholes, and the order and disorder of black hole information,” JHEP **08** (2020), 044 [arXiv:2002.08950](#) [hep-th].
- [38] T. J. Hollowood and S. P. Kumar, “Islands and Page Curves for Evaporating Black Holes in JT Gravity,” JHEP **08**, 094 (2020) [[arXiv:2004.14944](#) [hep-th]].
- [39] Y. Fan, N. Hunter-Jones, A. Karch and S. Mittal, “Sharp Transitions for Subsystem Complexity,” [arXiv:2510.18832](#) [hep-th].
- [40] J. Haah and D. Stanford, “Growth and collapse of subsystem complexity under random unitary circuits,” [[arXiv:2510.18805](#) [quant-ph]].
- [41] L. V. Iliesiu, A. Levine, H. W. Lin, H. Maxfield and M. Mezei, “On the non-perturbative bulk Hilbert space of JT gravity,” JHEP **10** (2024), 220 [[arXiv:2403.08696](#) [hep-th]].
- [42] A. Blommaert, C. H. Chen and Y. Nomura, “Firewalls at exponentially late times,” JHEP **10** (2024), 131 [[arXiv:2403.07049](#) [hep-th]].
- [43] D. Stanford and Z. Yang, “Firewalls from wormholes,” [[arXiv:2208.01625](#) [hep-th]].
- [44] P. Hayden and J. Preskill, “Black holes as mirrors: Quantum information in random subsystems,” JHEP **09** (2007), 120 [[arXiv:0708.4025](#) [hep-th]].
- [45] Y. Sekino and L. Susskind, “Fast Scramblers,” JHEP **10** (2008), 065 [[arXiv:0808.2096](#) [hep-th]].
- [46] L. Piroli, C. Sünderhauf and X. L. Qi, “A Random Unitary Circuit Model for Black Hole Evaporation,” JHEP **20** (2020), 063 [[arXiv:2002.09236](#) [hep-th]].
- [47] Z. Gyongyosi, T. J. Hollowood, S. P. Kumar, A. Legramandi and N. Talwar, “The holographic map of an evaporating black hole,” JHEP **07** (2023), 043 [[arXiv:2301.08362](#) [hep-th]].
- [48] J. M. Magan, M. Sasieta and B. Swingle, “Random circuits in the black hole interior,” SciPost Phys. **19** (2025) no.1, 007 [[arXiv:2412.08693](#) [hep-th]].
- [49] I.S. Gradshteyn, I.M. Ryzhik, D. Zwillinger and V. Moll, *Table of integrals, series, and products; 8th ed.*, Academic Press, Amsterdam (Sep, 2014), https://booksite.elsevier.com/samplechapters/9780123736376/Sample_Chapters/01-Front_Matter.pdf.
- [50] A. Blommaert and M. Usatyuk, “Microstructure in matrix elements,” JHEP **09** (2022), 070 [[arXiv:2108.02210](#) [hep-th]].
- [51] J. Kudler-Flam, V. Narovlansky and S. Ryu, “Distinguishing Random and Black

Hole Microstates,” PRX Quantum **2** (2021) no.4, 040340 [[arXiv:2108.00011](#) [hep-th]].

- [52] K. Okuyama, “Capacity of entanglement in random pure state,” Phys. Lett. B **820** (2021), 136600 [[arXiv:2103.08909](#) [hep-th]].